

Aus der Klinik für Gefäß-und Endovaskularchirurgie
der Heinrich-Heine-Universität Düsseldorf

Direktor: Univ.-Prof. Dr. Hubert Schelzig

**The role of osteopontin on stiffness related gene expression
in abdominal aortic aneurysms**

Dissertation

zur Erlangung des Grades eines Doktors der Medizin
der Medizinischen Fakultät der Heinrich-Heine-Universität
Düsseldorf

vorgelegt von
Yae Hyun Rhee
2023

Als Inauguraldissertation gedruckt mit Genehmigung der
Medizinischen Fakultät der Heinrich-Heine-Universität Düsseldorf

gez.:

Dekan: Prof. Dr.med. Nikolaj Klöcker

Erstgutachter: PD Dr.med. Markus Wagenhäuser

Zweitgutachter: Prof. Dr.rer.nat. Norbert Gerdes

코람 데오

Zusammenfassung

Das abdominale Aortenaneurysma (AAA) ist die Erweiterung des Aortenlumens um $\geq 50\%$ und wird durch eine Schwächung der Aortenwand verursacht. Das unbehandelte AAA ist mit einer hohen Rupturgefahr assoziiert, die eine hohe Sterblichkeit aufweist. Erhöhte Arteriensteifigkeit ist eine frühe Manifestation mikrostruktureller und funktioneller Veränderungen innerhalb der Aortenwand. In dieser Hinsicht kann insbesondere die segmentale Aortenversteifung (SAS) von aneinander angrenzenden Abschnitten zu einer AAA-Bildung beitragen, da die Perfusion und der zusammenhängende mechanische Stressverteilung in die Aortenwand nachteilig verändert wird. Dieses Phänomen fördert das AAA-Wachstum insbesondere in Regionen des Aortensteifigkeitsgradienten.

AAA enthält häufig einen intraluminalen Thrombus (ILT). Diverse Studien deuteten einerseits darauf hin, dass ein ILT einen biomechanischen Vorteil bieten kann, indem es die Belastung der Aortenwand verringert. Andere Studien hingegen verbanden eine Schwächung der Aortenwand aufgrund der durch den ILT erzeugten hypoxischen Verhältnisse in der Aortenwand. Auch wurde eine erhöhte proteolytische Aktivität innerhalb des ILTs selbst beschrieben.

Blutplättchen sind kleine Zellfragmente, die von Vorläufer-Megakaryozyten im Knochenmark stammen. Wenn aktiviert, setzen Blutplättchen verschiedene entzündungsfördernde Zytokine und andere biologische Modulatoren frei, die eine wesentliche Rolle bei verschiedenen entzündlichen und kardiovaskulären Erkrankungen spielen, unter anderem im AAA. Osteopontin (OPN) ist ein pro-inflammatorisches Zytokin, von dem vermutet wird, dass es zur Entwicklung und Progression von AAA beiträgt.

Diese Arbeit untersucht die Korrelation zwischen aktivierten Blutplättchen, OPN und seinen verschiedenen Fragmenten auf die Steifigkeits-assoziierte Genexpression in stationären und infiltrierenden Zellen der Aortenwand. Eine Alterierung dieses Expressionsmuster könnte die Entstehung und Progression eines AAA fördern.

Abstract

Abdominal aortic aneurysm (AAA) involves enlargement of the aortic lumen ($\geq 50\%$) and is caused by aortic wall weakening. Untreated AAA may rupture, which is associated with high mortality. Increased arterial stiffness is an early manifestation of microstructural and functional changes within the aortic wall. In this regard, segmental aortic stiffening (SAS) may trigger AAA formation and promote aneurysmal growth by altered blood flow and mechanical stress within the region showing an increased aortic stiffness gradient.

AAA is frequently accompanied by an intraluminal thrombus (ILT). Some studies suggest that ILT may provide a biomechanical advantage by decreasing aortic wall stress, whereas other studies have associated ILT with aortic wall weakening due to hypoxic conditions in the aortic wall and high proteolytic activity within the ILT.

Platelets are small cell fragments which derive from precursor megakaryocytes in the bone marrow. Once activated, platelets aggregate to form thrombus that resembles ILT in AAA lumen, release various pro-inflammatory cytokines and other biological response modulators, suggesting a pivotal role in various kinds of inflammatory and cardiovascular diseases, amongst others AAA. Osteopontin (OPN) is a well-known pro-inflammatory cytokine, which is secreted by pro-inflammatory cells such as macrophages and has been suggested to contribute to the development and progression of AAA.

This work investigated how activated platelets, OPN and OPN fragments in aortic cells correlate with the signaling pathways that affect aortic stiffness-related gene expression and contribute to AAA disease development.

Abbreviation

%	percent
°C	Celsius
β-ME	β-mercaptoethanol
μg	microgram
μl	microliter
μM	micromolar
AA	aortic aneurysm
AAA	abdominal aortic aneurysm
ADP	adenosine-5'-diphosphate
APS	activated platelet supernatant
BAPN	β-aminopropionitrile
BCA	Bicinchoninic Acid Protein Assay
BSA	bovine serum albumin
Ca	calcium
CaCl ₂	calcium chloride
CAVI	cardio-ankle vascular index
cDNA	complementary deoxyribonucleic acid
cf	'confer'
cm ²	square centimeter
COL1A1	human collagen type 1
COL3A1	human collagen type 3
CO ₂	carbon dioxide
COPD	chronic obstructive pulmonary disease
CRP	collagen-related-peptide
Cu	copper
CT	computed tomography
Ct	cycle threshold
CTA	computed tomography angiography
DMEM	Dulbecco's Modified Eagle Medium
DMSO	dimethyl sulfoxide
DNA	deoxyribonucleic acid
dNTP	deoxynucleotide triphosphate
DPBS	Dulbecco's Phosphate-Buffered Saline
ECM	extracellular matrix
EDTA	ethylenediaminetetraacetic acid

EVAR	endovascular aortic repair
FACS	fluorescence-activated cell sorting
FBS	fetal bovine serum
FL-OPN	full-length osteopontin
FSC	forward scatter
g	acceleration of gravity
GAG	glycosaminoglycan
GAPDH	glyceraldehyde-3-phosphate dehydrogenase
h	hour
H ₂ O	water
hAoF	human aortic fibroblast
hAoSMC	human aortic smooth muscle cell
HCl	hydrochloric acid
HuR	human antigen R
IFN	interferon
IL	interleukin
ILT	intraluminal thrombus
kDa	kilodalton
LPS	lipopolysaccharide
M	molar
MFI	mean fluorescence intensity
MgCl ₂	magnesium chloride
min	minutes
ml	milliliter
mM	millimolar
mm	millimeter
mm ²	square millimeter
MMP	matrix metalloproteinase
MMP-OPN	MMP cleaved osteopontin
MR	magnetic resonance
mU	milliunits
NaCl	sodium chloride
NaHCO ₃	sodium bicarbonate
ng	nanogram
NGAL	neutrophil-gelatinase-associated lipocalin
nm	nanometer
OD	optical density

OPN	osteopontin
OR	open surgical repair
PBS	phosphate buffered saline
PG	proteoglycan
PGE ₁	prostaglandin E1
PI-OPN	plasmin cleaved osteopontin
PMA	phorbol 12-myristate-13-acetate
PPE	porcine pancreatic elastase
PRP	platelet rich plasma
PTFE	polytetrafluoroethylene
PWV	pulse wave velocity
qPCR	real-time polymerase chain reaction
RNA	ribonucleic acid
RNase	ribonuclease
SAS	segmental aortic stiffness
SDS	sodium dodecyl sulfate
sec	seconds
SPP1	secreted phosphoprotein 1
SSC	side scatter
TAA	thoracic aortic aneurysms
TAAA	thoracoabdominal aneurysms
TEMED	tetramethylethylenediamine
TFP	thrombus formation potential
THP-1	human monocytic leukemia cell
TIMP	tissue inhibitor of metalloproteinases
TLR	toll-like receptor
TNF	tumor necrosis factor
Tr-OPN	thrombin cleaved osteopontin
Tris-HCl	hydroxymethyl aminomethane hydrochloride
U	units
V	volt
VSMC	vascular smooth muscle cell

Table of Contents

1. Introduction	1
1.1 Aortic aneurysm.....	1
1.1.1 Epidemiology	1
1.1.2 Risk factors.....	2
1.1.3 Etiology	2
1.1.4 Symptoms.....	4
1.1.5 Diagnostics	4
1.1.6 Therapy	5
1.1.7 Complications	6
1.2 Theories on AAA pathogenesis	6
1.2.1 Role of inflammation.....	7
1.2.2 Segmental vascular stiffness.....	7
1.2.3 Role of intraluminal thrombus (ILT)	8
1.2.4 Extracellular matrix (ECM) and matrix metalloproteinases (MMPs) 2, 9 ..	9
1.2.5 Osteopontin	12
1.3 Aim of the thesis	15
2. Materials and methods	17
2.1 Materials	17
2.1.1 Osteopontin and enzymes.....	17
2.1.2 Equipment	17
2.1.3 Consumables.....	18
2.1.4 Chemicals and reagents.....	18
2.1.5 Cell cultures.....	19
2.1.6 Cell culture media	20

2.1.7 Primer	20
2.1.8 Antibodies	21
2.1.9 Kits	21
2.1.10 Applied computer programs	21
2.2 Methods	21
2.2.1 Cell culture	21
2.2.2 Production of osteopontin fragments	25
2.2.3 Production of APS	29
2.2.4 Verification of platelet activation	30
2.2.5 Investigation of gene expression	31
2.2.6 Investigation of metalloproteinase activity	34
2.2.7 Statistics	37
3. Results	38
3.1 Stiffness related gene expression in response to APS exposure	38
3.1.1 M1-macrophages show the strongest OPN response to APS exposure	38
3.1.2 APS downregulates stiffness-related gene expression in hAoSMC and hAoF	39
3.1.3 APS upregulates OPN and MMP-9 gene expression in M1- macrophages	40
3.2 Effects of APS on MMP-9 activity	41
3.2.1 APS upregulates MMP-9 activity in M1-macrophages	41
3.3 Stiffness related gene expression in response to OPN treatment	43
3.3.1 MMP-2 gene expression is not regulated by OPN fragments in hAoSMC	43
3.3.2 Stiffness related genes are downregulated by OPN in hAoF	43

3.3.3 MMP-9 expression is not significantly regulated by OPN in M1- macrophages	44
3.4 Effects of OPN on MMP-9 activity	45
3.4.1 MMP-9 activity in M1-macrophages appears affected by long-term OPN exposure	45
4. Discussion	47
4.1 Effects of ILT and role of inflammation	49
4.2 Effects of ILT on ECM alteration.....	50
4.3 Effects of ILT and role of hypoxia	52
4.4 Effects of OPN on aortic stiffness: Alteration of ECM by MMP-2, -9	53
4.5 Effects of OPN on aortic stiffness: Collagen.....	56
4.6 Limitations	57
4.7 Conclusion.....	59
5. Bibliography.....	61

1. Introduction

1.1 Aortic aneurysm

Aortic aneurysm (AA) is a degenerative and progressive disease of the aortic wall with local dilatation of the aortic lumen $\geq 50\%$ of its original diameter. A dilatation $< 50\%$ of its diameter is considered a sub-aneurysmal aortic dilatation. As the growing size of the lumen bears a high risk of rupture, which is associated with high mortality, it is essential, once diagnosed, to diligently follow up over time in order to intervene prophylactically.

This work mainly explores the underlying mechanisms of abdominal aortic aneurysm (AAA) as it is the most commonly affected location, accounting for about 62.7% of all aortic aneurysms (1). Approximately 85% of these aneurysms occur below the renal arteries (2). Abdominal aortic aneurysms (AAA) can be subdivided into supra-, juxta- and infrarenal aneurysms depending on their location relative to the level of the renal arteries. AAA may also affect the iliac arteries (3).

1.1.1 Epidemiology

Screening programs in the United Kingdom and Sweden have estimated the prevalence of AAA at 1.3-1.9% among male patients (4), (5). However, the prevalence of AAA generally varies among different age classes and genders. Recent data from opportunistic screening during CT-colography or transthoracic echocardiography in New Zealand showed increasing prevalence of AAA with increasing patient age, and with higher prevalence in males than in females for all age groups (6), (7).

Age group	AAA prevalence (male patients)	AAA prevalence (female patients)
50-54	0.6 %	0.5 %
55-59	0.3 %	0 %
60-64	1.4 %	0.9 %
65-69	3.2 %	0.9 %
70-74	6.4 %	0.9 %
75-79	8.5 %	2.7 %
≥ 80	8.9 %	4.8 %

Recent studies postulate that the worldwide prevalence of AAA shows a decreasing trend. The Gloucestershire Aneurysm Screening Programme (GASP) published a decrease from 5% in 1991 to 1-3% in 2015 in ≥ 65 year-old men (8). Decreased smoking prevalence has been suggested to be primarily responsible. Other lifestyle influencing factors such as improved fitness and medical care-based cardiovascular risk reduction may also contribute to the decreasing AAA prevalence (8), (9), (10).

1.1.2 Risk factors

The main risk factor for AAA is aortic atherosclerosis that is closely linked to aging, renal hypertension, and nicotine consumption. In fact, smoking is the primary modifiable risk factor for AAA. Further, males and Caucasian people are more prone to develop AAA than women and people of other ethnicities. Patients suffering from cardiovascular comorbidities such as coronary heart disease and peripheral vascular disease are also at higher risk of AAA development. Further notable comorbidities are arterial hypertension and dyslipidemia (9), (11).

Minor risk factors include vasculitis of immunopathologic and infectious origin, connective tissue disorders such as Marfan, Loeys-Dietz and Ehlers-Danlos syndromes and cystic medial necrosis (Gsell-Erdheim disease). Positive family history is considered a major risk factor, accounting for 10% of AAA. Prevalence of 13% within families, and 25% among brothers has been recorded (12). Risk factors that may promote AAA rupture include female gender, diameter of AAA and active smoking.

1.1.3 Etiology

1.1.3.1 True vs. false Aneurysms

The aortic wall consists of three vessel layers: intima, media and adventitia. A true aneurysm results from the expansion of all three vessel layers. A false ('spurious') aneurysm is formed by a new (false) vascular lumen as a consequence of extraluminal bleeding. The wall of the 'pseudoaneurysm' originates from the reaction of the hematoma and surrounding connective tissue. Frequently, this type of aneurysm has a 'neck' between the affected artery and the aneurysm's lumen.

Dissecting aneurysms develop from previous aortic dissection. Dissection is a spontaneous tear of the intima with subsequent delamination of the media due to an intimal rupture.

1.1.3.2 Etiological classification

Degenerative

Degenerative aneurysms are the most common form of AA, and highly associated with atherosclerosis (13). Atherosclerosis may be caused by advanced age; however, tobacco smoking may be considered as the main risk factor along with smoking intensity and duration.

Other degeneration-associated factors include abnormal concentration of matrix metalloproteinases (MMP) which are responsible for extracellular matrix (ECM) remodeling and affect the vessel wall composition. Many of these enzymes gain or lose their function by posttranscriptional modifications. A deficit of anti-proteolytic enzymes which inhibit particularly MMP-1 may contribute to enhanced degenerative processes.

Inflammatory

(Chronic) inflammatory processes in the vessel wall may result in degeneration of the aortic wall and development of inflammatory aneurysms. Peri-vascular fibrosis is a consequence of inflammation. In axial CT-imaging, these aneurysms often appear with a thick inflammatory rind around the affected vessel. Representative diseases that may cause or are associated with inflammatory aneurysms include: Takayasu arteritis, Giant cell arteritis, Polyarteritis nodosa, Behçet disease, Cogan syndrome, and Cystic medial necrosis.

Traumatic

The most common cause of traumatic aneurysm is a local perforation of the aorta that results in a local hemorrhage with development of a false lumen and new luminal wall by the surrounding connective tissue (= "pseudoaneurysm").

Infectious

Infection of the aortic wall may derive from hematogenous spreading of germs or extension from adjacent structures around the external vessel tissue. Various organisms are known to be involved in aneurysmal disease such as tuberculosis,

syphilis, Candida and Aspergillus. Drug dependent and immunosuppressed patients are particularly vulnerable.

1.1.4 Symptoms

If not ruptured, most AAA are asymptomatic. In some cases, patients may complain about new onset of non-specific abdominal or lower back pain. In cases of rupture, patients describe sudden sharp back pain and present with hypovolemic shock symptoms.

1.1.5 Diagnostics

History taking includes questions about recent symptoms, cardiovascular risk factors, cardiac, respiratory and other comorbidities, family history and medication history. This information is essential for pre-surgical or -interventional risk stratification (14). During physical examination slim patients may demonstrate a pulsatile abdominal mass, most commonly supraumbilical.

At initial diagnosis, imaging is crucial. Ultrasonography is often used to characterize the morphology and measure the diameter. If an endoleak, defined as persistent blood flow outside of the stent graft into the aneurysmal sac, must be excluded for re-intervention, a contrast agent might be added. Ultrasonography has been approved as a method with affordable sensitivity and specificity. It saves radiation exposure compared to CT-angiography (CTA). However, diameter measurement may vary depending on the investigator and their technical skills. Further, ruptured aneurysms are rarely detected.

Angiography is not recommended as the first-step diagnostic tool for screening and surveillance due to its invasiveness. However, to plan for surgical repair of the aneurysm, a preoperative CTA with contrast medium is essential to visualize the location and morphologic characteristics of the aneurysm, which include aneurysm angulation, arterial tortuosity, arterial wall calcification and intravascular thrombus. Further, assessment of the aorta for a clamping zone (open repair) or landing zone of a stent graft (endovascular repair) is possible. CT imaging provides the whole aortic course, therefore concomitant aneurysms in the iliac or renal arteries can be

detected as well as arterial occlusive disease. It allows detection of atypical visceral arteries which are important for surgical planning. MR-angiography serves as an alternative, particularly if patients' renal function is impaired, and to avoid radiation. This diagnostic tool provides helpful information of the tissue status in case of inflammatory aneurysm. However, the assessment of wall calcification of the aorta may be challenging.

1.1.6 Therapy

To date, no pharmaceutical treatment is established for AAA development and growth prevention. Small aneurysms (< 5 cm) are therefore regularly monitored to thoroughly track the diameter growth. Surveillance is mainly performed by ultrasonography, or at wider intervals by contrast-medium-based CT-angiography. If the diameter exceeds 5 cm in females or 5.5 cm in male patients, prophylactic operative therapy is recommended to prevent spontaneous rupture of the aneurysm (14).

There are two surgical approaches available (13). Firstly, conventional open surgical repair (OR) is the traditional approach to eliminate AAA. Patients are placed under general anesthesia, and the aorta is exposed either via transperitoneal or retroperitoneal access. After systemic heparinization and identification of the proximal and distal clamping zones, the aorta is clamped. The aneurysm sac is opened by a longitudinal aortotomy and any intraluminal thrombus (ILT) is carefully removed prior to implanting a size-measured graft. ILT will be discussed more thoroughly in section 1.2.3. The graft material is either Dacron (textile polyester synthetic graft) or Polytetrafluoroethylene (PTFE, non-textile synthetic graft). After ensuring there is an appropriate blood flow through the graft, the anastomosis is completely closed, and the aneurysm sac closed to cover the graft.

In recent years, endovascular aortic repair (EVAR) has superseded OR due to its less invasive access via percutaneous transfemoral puncture, which avoids a laparotomy and the associated short and long-term complications which can have a significant impact on patients' general condition and recovery. After bilateral puncture, a catheter is inserted, and the wire cannulated at the aneurysm site under

the guidance of aortogram. Once the wire is correctly localized, the stent graft is inserted and expanded to be attached to the aortic wall. If aortoiliac stent graft is needed, the contralateral iliac graft is inserted before the ipsilateral. After ensuring of the absence of an endoleak (leaking of blood outside of the stent graft) and correct implantation of the stent graft with a final aortogram, the catheter and wire are removed, and the incision sutured.

1.1.7 Complications

The most severe complication of AAA is spontaneous rupture, which is associated with high mortality (15). In-hospital mortality was estimated at 53.1% in the USA and 65.9% in England (16). Acute mortality rate, defined as death before arrival at the next hospital or during the first admission, had been reported as high as 34% (17). According to a recent study by RESCAN collaborators, female patients had 4-fold higher rupture risk for all AAA sizes compared to men (18), (19). Further, the same study suggested that AAAs with larger diameter tend to grow faster. Whereas 3 cm diameter AAA featured 1.28 mm estimated growth/ year, 5 cm AAA was 3.61 mm/year. Lederle et al. reported <1% for 1-year-rupture incidence of small aneurysms (defined as < 5 cm). This risk increases exponentially with increasing size of the aneurysm diameter and exceeds 10% when the aneurysm is > 6 cm, but > 32.5% if > 7 cm (20). Growth rate is further enhanced in smokers resulting in double the rupture risk (18).

Annual risk of rupture of AAA

Size	1-year- incidence of rupture [%]
< 5.5 cm	≤ 1
5.5 – 5.9 cm	9.4
6.0 – 6.9 cm	10.2
≥ 7.0 cm	32.5

1.2 Theories on AAA pathogenesis

An important function of the arterial wall is to convert the highly pressured and pulsatile cardiac ejection of blood into moderated flow. This functionality depends on

the aortic wall structure, meaning that any structural change may affect the blood flow in the aorta, causing enhanced shear stress that favors aortic wall weakening and the development of an aneurysm.

The moderate fluctuation of blood flow is mainly regulated by an adequate ratio of collagen and elastin in the arterial wall. A major characteristic of AAA is the loss of elastin in the aortic wall along with enhanced apoptosis of vascular smooth muscle cells (VSMC). This section describes possible factors that are involved in structural alteration of the aortic wall.

1.2.1 Role of inflammation

Chronic inflammatory processes are considered to take a central part in aortic wall destruction (9). Aneurysmal tissues present infiltration of a wide range of innate and adaptive immune cells including macrophages, neutrophils, mast cells and T- and B lymphocytes. These cells enter the site of inflammation via vasa vasorum in the adventitia or from perivascular lymph nodes and release pro-inflammatory cytokines. Some macrophages may derive from trans-differentiation of local SMCs. Immune cells and the oxygen-derived radicals and cytokines, which they produce, can potentiate the induction of VSMC apoptosis and VSMC phenotype change that affect aortic medial wall structure. The release of proteases that can digest aortic wall structural components (such as microfibrils in the media) also eventually results in aortic wall fragmentation and wall thinning.

1.2.2 Segmental vascular stiffness

Chronic inflammatory processes along with enhanced activity of MMPs and subsequent degradation of elastin and collagen fibers in the aortic wall result in structural and functional changes in the aortic wall. Structural changes in AAA wall include overproduction of abnormal collagen and decreased elastin content.

Functional changes have been detected in patients with atherosclerosis-related AAA where significantly increased pulse wave velocity (PWV) and decreased arterial compliance have been measured (21).

Increased aortic wall stress contributes to AAA growth and increases the risk of

AAA rupture. Importantly, as AAA is primarily a condition of the elderly, aortic stiffening occurs with increasing age (an important risk factor). Defining segmental aortic stiffness (SAS) as the 'existence of a stiff aortic segment adjacent to a more compliant aorta', Raaz et al. introduced the idea that SAS contributes to AAA progression by augmented axial stress in the aortic wall (22). Elevated axial stress stimulates inflammation, leading to enhanced cytokine expression by and adhesion of inflammatory monocytes. Notably, vascular wall remodeling is also affected by increased VSMC apoptosis and enhanced activity of MMP-2 and -9; both result in loss of elastin content in the aortic wall, increasing aortic wall stiffening (22).

1.2.3 Role of intraluminal thrombus (ILT)

The majority (75%) of AAA contain ILT in the aneurysmal lumen (23). The formation of an ILT is suggested to result from the loss of elastin and subsequent decrease in longitudinal strength leading to elongation and tortuosity of major arteries. Due to the turbulent blood flow and low shear stress, endothelial injury is predilected with accumulation of platelets that increases the risk of thrombus formation in aneurysm (24), (25).

The majority of ILTs appear to be multi-layered, made of luminal, medial and abluminal layers (26). Usually, a liquid interphase can be found between the thrombus and the aneurysmal wall (27). The luminal layer mostly includes hematopoietic cells such as leukocytes, macrophages, erythrocytes, platelets and a dense fibrin network. The abluminal layer is in most cases devoid of cells but is marked by progressive fibrinolysis (28). It contains cellular components, and proteolytic proteins such as plasmin, MMPs and their tissue inhibitors are found in their inactive and active forms (29).

The role of ILT in aneurysm growth and rupture has been investigated, and correlations between the presence of ILT and aneurysm growth have been frequently reported (23), (30), (31), (32), (33), (34), (35), (36), (37). However, controversy exists in the literature regarding the effect of ILT on AAA. Some studies suggest a protective effect of ILT on AAA by reducing the wall stress and thus preventing rupture. Aneurysm rupture occurs when the local aortic wall stress

overcomes the aortic wall strength, and the ILT is described as a protective layer that absorbs the radial force of blood pressure, reducing the peak wall stress (34), (35), (38), (39), (40).

On the other hand, ILT can influence aneurysmal wall integrity in several ways. Containing various cellular components, the ILT has been described as a site of high biological activity since it is a source of storage, release and activation of various proteases (27), (29). In fact, a positive association between ILT thickness and AAA diameter has been reported in experimental rat models, suggested to be a result of increased biologic activity of ILT (29).

In this context, platelets may have a pivotal role in inducing inflammatory cascades and aortic wall destruction. Following vessel wall injury, activated platelets aggregate and form the first shape of a thrombus. During aggregation platelets degranulate and release pro-inflammatory chemokines as well as active proteases that had been stored in their inactive form in resting thrombocytes (41), and which then may affect aortic wall structure (23), (25), (27), (29), (42). Macrophages and neutrophils are recruited and trapped in the thrombus, enhancing the inflammatory cascade and releasing further pro-inflammatory cytokines such as interleukins (e.g. IL-6) and TNF- α . A canaliculi system within the ILT has been reported, suggesting a transport system of those macromolecules from the luminal side towards the vessel wall and affecting aortic wall metabolism (26), (28). The inflammatory environment contributes to the augmented synthesis and activation of proteolytic proteases, enhancing the degradation of the aortic wall and apoptosis of VSMCs. Consequently, explanted aortic aneurysmal tissues display thinner walls in the area which is covered by ILT, and contain less VSMC and elastin, resulting in decreased distensibility of the aorta (31).

1.2.4 Extracellular matrix (ECM) and matrix metalloproteinases (MMPs) 2, 9

The metabolism of ECM is regulated by continuous turnover of old and synthesis of new ECM components (43). Importantly, elastin and collagen are key structures for maintenance of aortic wall integrity. Well-known key enzymes that are responsible for ECM degradation are MMPs. MMPs are zinc-containing calcium-dependent

proteases and were first identified by their collagen proteolytic activity (44), (45). In addition to ECM metabolism, these enzymes are involved in modulating cell functions and signaling (46). Therefore, their activities are involved both in physiological processes such as angiogenesis and tissue remodeling as well as in multiple pathological diseases such as rheumatoid arthritis, various cancers with metastasis and cardiovascular diseases (45), (47). To date, up to 28 members of MMP family have been found in vertebrates, 23 of which are expressed in human tissues, and 14 of those are found in vasculature (45), (48).

These enzymes are expressed as inactive pre-proenzymes. The signal peptide is removed post-translationally which converts them to inactive proenzymes. Active enzymes gain their final function by cleavage of the cysteine switch and the detachment of the pro-peptide domain by other proteolytic enzymes such as serine proteases, the endopeptidase furin, plasmin, or other MMPs. Their activity is further regulated by endogenous tissue inhibitors of metalloproteinases (TIMP). TIMPs are able to inhibit both active MMPs by binding in a 1:1 stoichiometry, and by preventing activation of pro-MMPs (45), (49). There are four identified TIMPs which are labeled TIMP-1, -2, -3 and -4. The ratio of MMP to TIMP is essential for sustaining the balance of ECM production and degradation.

Based on their substrates and the organization of their structural domains, MMP enzymes are categorized into 6 groups: collagenases, gelatinases, stromelysins, matrilysins, membrane-type MMPs, and others. The present work mainly focuses on gelatinase A (MMP-2) and gelatinase B (MMP-9), since elevated serum levels of MMP-2 and -9 (0.06–0.6 μ g/mL) have been found in AAA patients along with enhanced MMP activity in aortic tissue (50). Further, histologic examinations of AAA tissue indicate enhanced degradation of elastin lamellae in the media and increased amounts of immature collagen type I and III which indicate disturbed ECM metabolism, which results in subsequent aortic wall weakening, dilatation and development of AAA. Studies have shown that MMP-2 (72 kDa) is mainly expressed by resident aortic cells such as vascular smooth muscle cells (VSMC) and fibroblasts, and has the greatest elastolytic activity (51). It is also known to degrade various collagen types including I and III. MMP-2 expression in VSMC is augmented in close

proximity to pro-inflammatory cells suggesting that these inflammatory cells provide stimulating factors e.g., pro-inflammatory cytokines.

MMP-9 (92 kDa) was concomitantly identified with pro-inflammatory cells such as M1-macrophages and neutrophils in AAA tissue (25), (52). A relation between aneurysm size and MMP-9 concentration has been proposed, suggesting higher concentrations are found in bigger aneurysms (53). Furthermore, higher concentrations of MMP-9 have been detected in patients with ruptured AAA (54). Notably, serum levels of MMP-9 decrease shortly after aneurysm repair (55). Sangiorgi et al. found that elevated MMP-9 in plasma has 48% sensitivity and 95% specificity as a diagnostic screening test for AAA in a meta-analysis including 580 AAA cases and 258 controls (56). However, data in subsequent studies have shown a non-significant correlation between levels of MMP-9 and AAA diameter or between the plasma and aneurysm wall levels of any MMP or TIMP, and AAA diameter (45). Additionally, the negative predictive value was too high (52%) to establish MMP-9 as a reasonable screening marker.

On the cellular level, MMP-2 and -9 may play a role in inhibitory modulation of Ca^{2+} dependent aortic VSMC contractility. The contractility of aortic smooth muscle cells is important to maintain the integrity of aortic wall against the pulsatile blood flow generated by each cardiac ejection. The inhibitory effects of MMP-2 and -9 may add to further weakening of the aortic wall (49), (57).

Under physiological conditions, MMPs regulate the growth, proliferation and migration of VSMC by providing cleaved growth factors to cells that are not in direct contact with the ECM. However, when expressed in excess, MMPs promote VSMC apoptosis by degrading ligands such as TNF- α and Fas ligand. Experimental induction of aortic aneurysm provides evidence that MMPs are essential in developing aortic aneurysms. Studies with knock-out mice of MMP-2 and -9 resulted in impaired aneurysm formation in murine aorta. A suggested hypothesis is that MMP-2, as a primary collagenase, initiates cleavage of triple-helical collagen generating single α chains. These could then be further processed by MMP-9, releasing coiled elastin. In summary, MMP-2 and -9 likely work in concert in the development of aortic aneurysm (58), (59).

1.2.5 Osteopontin

Osteopontin (OPN) is a highly acidic multi-functional glycoprotein, which was first called secreted phosphoprotein 1 (SPP1), and identified from malignantly transformed mammalian cells by Senger et al in 1979 (60), (61). Human osteopontin is about 32 kDA and undergoes various post-translational modifications including phosphorylation, glycosylation, sulfation and transglutamination resulting in size ranging from 44-75 kD (62), (63), (64), (65), (66), (67). This protein participates in many physiological processes, and is mainly expressed in bone and epithelial surfaces including respiratory, reproductive and urinary tract as well as mammary epithelium (62). Secreted by osteoclasts and osteoblasts, OPN plays an important role in bone remodeling and bone calcification. Secondly, it is secreted by pro-inflammatory cells, particularly macrophages and T-cells, and is involved in inflammatory responses as a cytokine.

Chronic inflammation, atherosclerosis and proteolysis are important factors in the pathogenesis of AAA. An elevated tissue concentration of OPN was consistently observed in AAA patients' aortic biopsies. The significance of OPN in AAA disease was first reported by Golledge et al. in 2007 (68). The study describes that, after adjusting for other risk factors for AAA, OPN was an independent AAA-associated factor. Patients with elevated OPN concentrations were twice as likely to have AAA. Further serum OPN was positively correlated with aneurysmal growth. However, the sensitivity (73%) and specificity (52%) were too low to establish the protein as a screening marker. Experimental studies with ApoE/OPN double knock-out mice presented an association of OPN in AAA development since the knockout mice were protected against AAA formation (69).

Supporting inflammatory mechanisms within the development of AAA, OPN promotes macrophage and T-cell chemotaxis and adhesion, and prolongs lymphocyte survival, which as a package augments cell-mediated immune response. Moreover, it is known to be a substrate for MMPs, thereby playing an important role in ECM remodeling and degradation in the aortic wall.

Cellular processes are mediated through interactions with CD44 and a number of

integrin receptors including $\alpha_4\beta_1$, $\alpha_5\beta_1$, $\alpha_8\beta_1$, $\alpha_8\beta_1$, $\alpha_9\beta_1$, $\alpha_v\beta_1$, $\alpha_v\beta_3$, $\alpha_v\beta_5$ and $\alpha_v\beta_6$ on the cell surface. OPN can either interact in its full-length form (FL-OPN) via RGD sequence (amino acids Arginine-Glycine-Aspartic acid) or after cleavage by proteolytic enzymes, with its fragments serving as interacting ligands. In addition to MMPs (MMP-2, -3, -7, -9, -12), thrombin, plasmin and cathepsin D can cleave OPN, all generating different OPN fragments. Varying affinities to certain integrins between full length OPN (FL-OPN) and OPN fragments has been reported depending on the structure of the protein, suggesting significant implications for subsequent cellular processes of different OPN fragments (66), (67), (70).

Thrombin cleaves full-length OPN into two fragments (Tr-OPN) with similar molecular weights of around 30 kDa. The cleavage site is between ¹⁵²R and ¹⁵³S which exposes cryptic N-terminal SVVYGLR (Ser-Val-Val-Tyr-Gyl-Leu-Arg) sequence adjacent to an RGD motif (67). The cryptic N-terminal SVVYGLR favorably binds to $\alpha_4\beta_1$ and $\alpha_9\beta_1$, resulting in enhanced cell migration and proliferation.

Plasmin's major cleavage site includes two amino acids at the C-terminal thrombin cleavage site of OPN. The preferred amino acids were identified to be lysine or arginine residues. Equally strong affinity to $\alpha_v\beta_3$ and $\alpha_5\beta_1$ as Tr-OPN was detected, and mediates cellular adhesion (67).

MMP-3 and -7 cleave within the ¹⁶²SVVYGLR¹⁶⁸ motif, preferably between Glycine and Leucine, generating fragments between 25 and 40 kDa (71). These fragments are reported to play a significant role in increased tumor cell adhesion and peritoneal macrophage migration. Two predominant MMP-9 cleavage sites have been explored by Takafuji et al. proposing four fragments with sizes of 5, 24, 32, and 34 kDa. In particular, the 5 kDa fragment has been suggested to enhance tumor metastasis via interaction with the CD44 receptor (72). MMP-2 cleaves OPN into two 20 kDa major fragments (46). Exact cleavage sites have not yet been discovered.

OPN and its fragments may be involved in activation and upregulation of MMPs by means of a positive feedback loop. Philip et al. reported the capability of OPN to activate pro-MMP-2 through nuclear factor κ B-mediated signaling in murine melanoma cells (73). A study by Gao et al. found that OPN induces the expression of MMP-2 which in turn results in increased OPN activity (66). Supporting evidence

was introduced by Seo et al. showing in their in vitro and in vivo studies that VSMC expressed increased levels of OPN and MMP-2 when exposed to mechanical stretch, mimicking arterial hypertensive disease. OPN also displayed an autocrine function such that, when secreted into the ECM, it contributed to enhanced production and activity of MMP-2 via CD44 receptor interaction (74).

1.3 Aim of the thesis

Despite extensive research regarding AAA pathology, there is currently no effective medical treatment available to prevent aneurysm development, growth and rupture. Open surgical or endovascular repair are the only therapeutic options, are only available to those patients with large aneurysms, and present significant surgical risks. Patients with small aneurysms are only monitored at regular intervals, which is correlated with an impaired quality of life (43). Further, AAA is commonly found in aged patients who have augmented risk for surgical complications. Administration of doxycycline in in vitro SMC culture experiments and in vivo models had been reported to be a potent MMP expression inhibitor and suggested as pharmaceutical treatment (58), (75), (76). However, due to its heavy side effects and adverse efficacy in clinical trials, the treatment could not be established (9).

This project aims to investigate the correlation between the presence of ILT and activation of MMPs, resulting in OPN-mediated regulation of stiffness-related gene expression in AAA pathology, with the following two theses.

- 1) Multiple studies have shown that large aneurysms are accompanied by ILT. ILT is known as a site of highly active inflammatory processes that affect ECM remodeling of the aortic wall. A pivotal role has been attributed to OPN, which is found to be elevated in AAA patients and contributes to AAA progression (68).

We are interested in which aortic cell type mainly produces OPN after contact with activated platelet supernatant (APS). Target cell lines are pro-inflammatory M1-macrophages, human aortic smooth muscle cells and human aortic fibroblasts.

- 2) Activated platelets are not only involved in inflammatory processes but appear to additionally affect ECM remodeling of the aortic wall by actively releasing and activating ECM-degrading enzymes. Higher concentrations of plasmin and thrombin in ILT compared to aortic wall have been reported which

interestingly can cleave OPN (29), (41), (77), (78). Chronic enhanced inflammation and ECM remodeling result in arterial stiffening that contributes to AAA progression.

We hypothesize that elevated FL-OPN and OPN fragments have impacts on stiffness-related gene expression (collagen types I and III, MMP-2 and -9) and MMP activity in inflammatory and aortic resident cells involved in AAA pathology.

2. Materials and methods

2.1 Materials

2.1.1 Osteopontin and enzymes

human recombinant osteopontin 50 µg, 250 µg Lot# 1108467	Peprotech, New Jersey, USA
plasmin Lot# SLBZ9079	Sigma-Aldrich, Missouri, USA, Steinheim, Germany
thrombin Lot# 21637823	Sigma-Aldrich, Indianapolis, USA

2.1.2 Equipment

aspiration system	Vacusaft, Integram Biebertal, Germany
centrifuge	Heraeus Megafuge 40 R Thermo Fisher Scientific, Waltham, USA
electrophoresis cell	Mini-PROTEAN® Tetra Electrophoresis Cell, Bio-Rad, Hercules, USA
flow cytometer	FACSCalibur™, BD Sciences, Heidelberg, Germany
freezer -20 °C	Liebherr, Biberach an der Riß, Germany
freezer -80 °C	Thermo Fisher Scientific, Waltham, USA
fridge 4 °C	Liebherr, Biberach an der Riß, Germany
haemocytometer	Neubauer Counting Chamber Hecht-Assistent, Sondheim v. d. Rhön, Germany
hematology analyzer	KX-21N, Sysmex Europe GmbH, Norderstedt, Germany
incubator	HeraCell 240 Heraeus, Hanau, Germany
isopropanolol freezing container	Nunc, Sigma-Aldrich, Munich, Germany
microscope	CKX41 Olympus, Hamburg, Germany
molecular imager	ChemiDoc™ MP System Bio Rad, Hercules, USA
nitrogen tank -160 °C	Thermo Fisher Scientific, Waltham, USA
pH-Meter	FE20 Mettler Toledo, Gießen, Germany
platform shaker	Duomax 1030 Heidolph Instruments, Schwabach, Germany

power supply	PowerPac™ Basic Power Supply, Bio-Rad, Hercules, USA
qPCR machine	Bio-Rad Model CFX96 Optical Reaction Module, Hercules, USA
safety cabinet	Safe 2020 Thermo Fisher Scientific, Waltham, USA
scale	Extend Sartorius, Sartorius AG, Göttingen, Germany EK 3000i, A&D Company, Tokyo, Japan
spectrophotometer	Nanodrop 2000c, PEQLAB/VWR, Darmstadt, Germany
vortex mixer	Vortex-Genie 2, Scientific Industries, Bohemia, USA
water bath	Wine One, Memmert, Schwabach, Germany

2.1.3 Consumables

cell culture flask T175, T75	Sarstedt, Nümbrecht, Germany
cell culture plate 12-, 24-, 96-well	Greiner Bio-One, Frickenhausen, Sarstedt, Nümbrecht, Germany
cryotubes 2 ml	Greiner Bio-One, Frickenhausen, Germany
disposable gloves	Ansell, Brussels, Belgium
disposal bags	Carl Roth, Karlsruhe, Germany
facial tissue	Tapira, Heidenheim, Germany
conical centrifuge tubes 15, 50 ml	Corning, New York, USA
Parafilm	Bemis Corporate, Neenah, USA
pipettes 0,5-10, 10-100, 100-1000 µl	Research plus Eppendorf, Hamburg, Germany
motorized pipette controller	Easypet Eppendorf, Hamburg, Germany
motorized pipette controller	Pipetus Hirschmann, Eberstadt, Germany
reaction tubes 1,5 ml, 2 ml	Sarstedt, Nümbrecht, Germany
serological pipets 5, 10, 25 ml	Corning, New York, USA
sterile pipet tips 10, 100, 1000 µl	Starlab, Hamburg, Germany
sterile spatula	B. Braun AG, Melsungen, Germany

2.1.4 Chemicals and reagents

adenosine-5'-diphosphate (ADP)	Sigma-Aldrich GmbH, Steinheim, Germany
--------------------------------	--

ammonium bicarbonate	Sigma-Aldrich GmbH, Steinheim, Germany
apyrase	Sigma A7646 GmbH, Steinheim, Germany
Brij-35	Carl Roth, Karlsruhe, Germany
calcium chloride (CaCl ₂)	VWR International, Radnor, Pennsylvania, USA
calibration solution pH 7.01/4.01/10.01	Hanna Instruments, Woonsocket, USA
collagen-related peptide (CRP)	Department of Biochemistry, University of Cambridge, UK
Dimethyl sulfoxide (DMSO)	Merck, Darmstadt, Germany
Dulbecco's Phosphate-Buffered Saline (DPBS)	Thermo Fisher Scientific, Waltham, USA
Dulbecco's Modified Eagle Medium (DMEM; 10 x)	Life Technologies GmbH, Darmstadt, Germany
ethanol 70 %, 96%	VWR International, Radnor, Pennsylvania, USA
fibroblast basal medium 2 kit	PromoCell GmbH, Heidelberg, Germany
fetal bovine serum (FBS)	PAN- Biotech, Aidenbach, Germany
gentamycin 10 mg/ml	Biochrom, Berlin, Germany
glutamine 200 mM	Biochrom, Berlin, Germany
hydrochloric acid (HCL)	Merck, Darmstadt, Germany
hydroxymethyl aminomethane hydrochloride (Tris-HCl)	Sigma-Aldrich GmbH, Munich, Germany
interferon gamma (IFN- γ)	Sigma-Aldrich, GmbH, Munich, Germany
lipopolysaccharide (LPS)	Sigma-Aldrich, GmbH, Munich, Germany
penicillin/streptomycin	Thermo Fisher Scientific, Waltham, USA
phorbol 12-myrystate-13-acetate (PMA)	
PowerUp™ SYBR™ Green Master Mix	Thermo Fisher Scientific, Vilnius, Lithuania
Roswell Park Memorial Institute Medium 1640 (RPMI; 1x)	Life Technologies GmbH, Darmstadt, Germany
sodium bicarbonate (NaHCO ₃)	Biochrom, Berlin, Germany
sodium chloride (NaCl)	Carl Roth, Karlsruhe, Germany
TRizol™ Reagent	Thermo Fisher Scientific, California, USA
trypan blue 0.4 %	Sigma-Aldrich GmbH, Munich, Germany
trypsin 0.25 %	Biochrom, Berlin, Germany
zymogram development buffer (10x)	Bio-Rad, Hercules, USA

2.1.5 Cell cultures

human aortic fibroblasts	PromoCell, Heidelberg, Germany
human aortic smooth muscle cells	PromoCell, Heidelberg, Germany

human monocytic leukemia cells	DSMZ, Braunschweig, Germany
--------------------------------	-----------------------------

2.1.6 Cell culture media

Human aortic fibroblast (hAoF)

Fibroblast basal medium 2 kit

basal medium 500 ml

FBS 0.02 ml/ml

human recombinant Insulin (5 µg/ml)

human recombinant basic fibroblast growth factor (1 ng/ml)

Human aortic smooth muscle cell (hAoSMC)

Dulbecco's Modified Eagle Medium (DMEM) 500 ml

+ 4,5g/L D-Glucose, L-Glutamine

+ 1% Penicillin-Streptomycin

+ 20% FBS

Human monocytic leukemia cell (THP-1)

RPMI 1640 medium 500 ml

+ L-Glutamine

+ 1% Penicillin-Streptomycin

+ 10% FBS

2.1.7 Primer

Name of RT ² qPCR Primer Assays	Catalog Number	Order Number	Company
Glycerinaldehyde-3-phosphate dehydrogenase (GAPDH)	33001	PPH00150F	Qiagen GmbH, Hilden, Germany
Human osteopontin (SPP1)	33001	PPH00582E-200	Qiagen GmbH, Hilden, Germany
human matrix-metalloproteinase 2 (MMP2)	33001	PPH00151B	Qiagen GmbH, Hilden, Germany
human matrix-metalloproteinase 9 (MMP9)	33001	PPH00152E	Qiagen GmbH, Hilden, Germany

human collagen type I (COL1A1)	33001	PPH01299F	Qiagen GmbH, Hilden, Germany
human collagen type III (COL3A1)	33001	PPH00439F	Qiagen GmbH, Hilden, Germany

2.1.8 Antibodies

Name	Company
CD61-PE	BD Biosciences, Heidelberg, Germany
CD62P-PE	BD Biosciences, Heidelberg, Germany
PAC1-FITC	BD Biosciences, Heidelberg, Germany

2.1.9 Kits

cDNA high-capacity reverse transcription kit	Applied Biosystems, Foster City, USA
Pierce™ silver stain kit	Thermo Fisher Scientific, Rockford, USA
RNeasy® Mini Kit	Qiagen GmbH, Hilden Germany

2.1.10 Applied computer programs

Graph Pad Prism 8	GraphPad Software, San Diego, USA
Image Lab	Bio-Rad, Hercules, USA
Mendeley Elsevier-Reference Management Software	London, UK
Microsoft Word 2016	Microsoft, Redmond, USA
Microsoft Excel 2016	Microsoft, Redmond, USA

2.2 Methods

2.2.1 Cell culture

2.2.1.1 General information

Human cell lines (THP-1) and primary human cells (hAoF, hAoSMC) were utilized for *in vitro* experiments in a sterile biosafety cabinet according to standards of operation. Cells were cultured in an incubator under the following conditions, if not otherwise mentioned.

temperature 37 °C

carbon dioxide (CO₂) concentration 5 %

humidity 95 %

Cell media, buffers and liquid supplies were briefly heated in a water bath at 37 °C prior to utilization. Cell pellets from cell suspensions were generated by centrifugation at 26 °C and 200 x g for 5 minutes.

2.2.1.2 Cell cultivation

Frozen cell aliquots were marginally defrosted in a water bath at 37 °C. The pellet was transferred into a tube filled with 12 ml of warm cell media and gently dissolved. The cell suspension was transferred into a T75 cell flask (hAoSMC, THP-1) or 10 mm Petri dish (hAoF) to grow the cells in the incubator at 37 °C overnight. Cell media was replaced on the following day to wash out DMSO. Media replacement took place every three to five days. The cells were cultivated up to 70-80% of confluency before passaging.

Passaging adherent cells

To dissolve the intercellular and the cell-dish surface connections, cells were washed once with pre-warmed sterile PBS and treated with 2 ml trypsin/EDTA (1%) at 37 °C. After 3-5 minutes incubation, cell detachment was confirmed by microscopy. For neutralization 8 ml of fresh media was added. The cell suspension was centrifuged to obtain a cell pellet. The supernatant was discarded, the cell pellet was solved in fresh media and seeded in new flasks (hAoSMC; 175 cm²) or dishes (hAoF; 10 mm). The average cell number was 1 x 10⁵ cells/mm².

Passaging Suspension cells

Suspension cells were transferred into a 15 ml tube before they were centrifuged to obtain a cell pellet. After removing the supernatant, the cell pellet was washed once with 10-15 ml pre-warmed sterile PBS and centrifuged again. Thereafter, the supernatant was discarded, and the cell pellet was resuspended in fresh media before cells were transferred into a new flask (175 cm²).

2.2.1.3 Cell counts

Prior to cell counting, cells were dissolved from the flask/dish as described previously to obtain a cell pellet which was resuspended in fresh media multiple times. Out of the cell suspension 20 µl was taken and mixed with trypan blue at the rate of 1:1.

Since this chemical dye is not able to penetrate an intact cell membrane, dead cells are colored blue which can be detected under the microscope. To gain the total number of cells per ml, 10 μ l sample of the suspension was put into a Neubauer counting chamber and cells in 4 large squares were counted under the microscope. According to the formula below, the total number of cells can be calculated as follows:

$$\text{cells/mL} = \left(\frac{(\text{number of cells counted})(\text{dilution factor})}{(\text{number of large squares counted})(\text{volume of 1 large square})} \right) \times 10000$$

Number of large squares counted= 4

Dilution factor=2

2.2.1.4 Differentiation of M1-macrophages

For M1-differentiation a modified protocol by Park et al. (79) was applied. THP-1 cells were seeded in 24-well plates for differentiation, each well containing 1.5×10^5 cells. On seeding, cell media was enriched with 5 ng/ml PMA and cells were incubated for 48 h at 37 °C to be differentiated to M0-macrophages. Cell media was replaced by new media including 100 ng/ml LPS and 20 ng/ml IFN- γ to induce the final differentiation to M1-macrophages for 24 h.

2.2.1.5 Interaction of activated platelet supernatant (APS) and aortic cells

To achieve 80-90 % of confluency resident aortic cells (hAoF and hAoSMC) were seeded 1.5×10^5 per well in 12-well plates 24 h prior to the beginning of the experiment. The inflammatory M1-macrophages were seeded 1.5×10^5 per well in 24-well plates as mentioned above.

The media was removed, and cells were washed once with 700 μ l sterile PBS. After removing PBS, cells were treated with APS according to the following pipetting scheme. To obtain variation in the platelet supernatant, four to five patients' blood samples were pooled. APS control cells were treated with Tyrode buffer (an isotonic solution to protect the cells from dehydration) only (plain or activated) to maintain the difference of treatments in the absence or presence of platelets. The incubation time was set to 6 h for short- and 24 h for long-term treatments.

Control 1	Control 2	Control 3	Control 4
CRP Control 1	CRP Control 2	CRP Control 3	CRP Control 4
ADP Control 1	ADP Control 2	ADP Control 3	ADP Control 4

Resting 1	Resting 2	Resting 3	Resting 4
CRP APS 1	CRP APS 2	CRP APS 3	CRP APS 4
ADP APS 1	ADP APS 2	ADP APS 3	ADP APS 4

Control: Cells are treated with 50% Tyrode and 50% cell media
CRP control: Cells are treated with 50% Tyrode (incl. 10% CRP) and 50% cell media
ADP control: Cells are treated with 50% Tyrode (incl. 10% ADP) and 50% cell media
Resting: Cells are treated with 50% non-activated platelet supernatant and 50% cell media
CRP APS: Cells are treated with 50% CRP-activated platelet supernatant and 50% cell media
ADP APS: Cells are treated with 50% ADP-activated platelet supernatant and 50% cell media

Cells were harvested after the aforementioned period of time. Non-sterile PBS was stored on ice for 20 minutes prior to harvest. The supernatant was removed, and resident cells were washed with 900µl/well and the inflammatory cells with 500 µl/well ice-cold PBS twice to three times, respectively.

Cells were homogenized with 700 µl (12-well plates) or 500 µl (24-well plates) TRIzol™ reagent respectively to extract RNA in the following steps. The lysate was transferred to 1.5 ml tubes and chloroform added at the rate of 1 (chloroform) : 5 (TRIzol™). After 3 minutes of incubation the samples were centrifuged at 12 000 x g for 15 minutes at 4 °C. To isolate cellular RNA, only the upper aqueous phase was aspirated and transferred to new tubes for further processing.

2.2.1.6 Interaction of osteopontin fragments and aortic cells

To achieve 80-90% confluency, resident aortic cells (hAoSMC, hAoF) were seeded 1.5×10^5 per well in 12-well plates 24 h prior to the beginning of the experiment. Inflammatory M1-macrophages were seeded 1.5×10^5 per well in 24-well plates as mentioned in 2.2.1.4. Each experiment included an average number of 4-6 samples. The media was removed, and cells were washed once with 700 µl/well sterile PBS. After removing PBS, cells were treated according to the following pipetting scheme. Similar to APS controls, OPN fragment control cells were treated with enzymes in enzyme buffer to maintain the same conditions as much as possible and to subtract the effects of the enzymes in the subsequent calculation. The incubation time varied between 6 and 24 h to investigate both short- and long-term treatment effects.

Plate 1

Control 1	Control 2	FL-OPN 1	FL-OPN 2
Control 3	Control 4	FL-OPN 3	FL-OPN 4
Control 5	Control 6	FL-OPN 5	FL-OPN 6

Plate 2

Thrombin Control 1	Thrombin Control 2	Tr-OPN 1	Tr-OPN 2
Thrombin Control 3	Thrombin Control 4	Tr-OPN 3	Tr-OPN 4
Thrombin Control 5	Thrombin Control 6	Tr-OPN 5	Tr-OPN 6

Plate 3

Plasmin Control 1	Plasmin Control 2	PI-OPN 1	PI-OPN 2
Plasmin Control 3	Plasmin Control 4	PI-OPN 3	PI-OPN 4
Plasmin Control 5	Plasmin Control 6	PI-OPN 5	PI-OPN 6

Control: Cells were treated with 100 % cell media.

Thrombin control: Cells were treated with 98 % cell media and 2 % activated thrombin in ammonium bicarbonate buffer.

Plasmin control: Cells were treated with 98 % cell media and 2 % activated plasmin in ammonium bicarbonate buffer.

Tr-/PI-OPN: Cells were treated with 98 % cell media and 2 % osteopontin fragments in ammonium bicarbonate or development buffer, respectively.

The process of cell harvesting followed the methods mentioned already above.

2.2.2 Production of osteopontin fragments

Osteopontin fragments were produced by applying modified protocols by Christensen et al. (67) and Agnihotri et al. (71). Briefly, incubation buffers were prepared for thrombin/plasmin and the matrix metalloproteinases prior to the fragmentation.

The ammonium bicarbonate buffer included:

ammonium bicarbonate	0.1 M
distilled H ₂ O	

MMP specific development buffer (pH 7.5) included:

Tris HCl	50 mM
CaCl ₂	5 mM
NaCl	200mM

Brij-35	0,02%
---------	-------

For the fragmentation of FL-OPN, 1 µg human recombinant osteopontin was incubated with various enzymes mentioned below for a defined period of time. Osteopontin fragments were detected by silver staining. The fragments were stored at -20 °C until use.

Thrombin cleaved osteopontin (Tr-OPN): incubation for 3 h at 37 °C

- 1) 1 µg FL-OPN
- 2) 30 mU human recombinant thrombin
- 3) 0.1 M ammonium bicarbonate buffer

Plasmin cleaved osteopontin (Pl-OPN): incubation for 3 h at 37 °C

- 1) 1 µg FL-OPN
- 2) 15 mU of human recombinant plasmin
- 3) 0.1 M ammonium bicarbonate buffer

Enzyme controls

OPN cleaving enzymes (thrombin and plasmin) were incubated in ammonium bicarbonate/MMP-specific development buffer respectively without OPN for the same period of time as mentioned above at 37 °C. Controls were required to distinguish between enzyme effects and OPN effects on cells.

2.2.2.1 Silver Stain

Silver stain is a sensitive colorimetric method to detect proteins. For this method the Pierce™ Silver Stain Kit was utilized according to the manufacturer's protocol (Thermo Fisher Scientific, USA). The principle of staining "involves the deposition of metallic silver onto the surface of a gel at the locations of protein bands." Silver ions of the staining reagent interact with functional groups of the protein in the sample. During the developing process the silver ions are chemically reduced to metallic silver which is visible as brown-black color on the gel.

In detail, samples of FL-OPN and various OPN fragment samples were centrifuged briefly to spin down the contents. Laemmli buffer (1.5 M Tris-Cl, glycerol, β-mercaptoethanol, SDS, 1% bromophenol blue) was diluted to a quarter concentration and added to the sample. The solution was heated at 95 °C for 5 min

to linearize the protein structure. The final volume of 20 µl of each sample was loaded on a 15% SDS-PAGE gel.

Separating gel: final concentration of polyacrylamide is 15 %

components	volume
lower buffer (1,5M Tris base 0,4% SDS; pH 8.8)	5 ml
30% acrylamide	10 ml
distilled H ₂ O	4.89 ml
10% ammonium persulfate	0.10 ml
tetramethylethylenediamine (TEMED)	0.01 ml

Stacking gel: final concentration of polyacrylamide is 4.5 %

components	volume
upper buffer (0,5M Tris base, 4% SDS; pH 6.8)	0.84 ml
30% acrylamide	0.5 ml
distilled H ₂ O	1.96 ml
10% ammonium persulfate (APS)	0.033 ml
TEMED	0.003 ml

When preparing the gels, TEMED and ammonium persulfate were added shortly before pouring. After composing the mixture without ammonium persulfate and TEMED, the solution was mixed thoroughly on a magnet stirrer. Ammonium persulfate and TEMED were added just before pouring the solution into the chamber, leaving ¼ space on the top. The top is layered with 70 % ethanol to create a straight lane. The gel was completely polymerized after about 30 min incubation.

In the meantime, the stacking gel was prepared according to the composition list above. Subsequently, the gel was poured on top of the separating gel after removing 70 % ethanol, and a well comb was added. After 30 min incubation the gel was polymerized. For the complete polymerization the gels were stored at 4° C until use, and then incubated at room temperature just prior to use.

The gel was clamped into the apparatus and both buffer chambers were filled with running buffer. After loading the samples, one well of each gel was loaded with a ladder to identify the molecular weight of separated protein bands. A forerun phase

was started at 90 V for 10 min which was followed by 70 min running time at 120 V. After the electrophoresis, the gel was washed twice with 100 ml ultrapure water for 5 min and incubated in a fixing solution for 30 min in total. The fixing solution contained ethanol, acetic acid and water at a ratio of 6:3:1 and was replaced after the first 15 min. Thereafter, the gel was washed twice in 10% ethanol solution for 5 min and afterwards then twice in ultrapure water for further each 5 min. After washing, the gel was incubated in sensitizer working solution (1 silver stain sensitizer:500 ultrapure water) for 1 min and washed with two changes of ultrapure water for each 1 min. For the staining process a stain working solution was prepared with silver stain enhancer and silver at a ratio of 1:50 and the gel incubated for 30 min at room temperature.

After incubation the gel was washed twice in ultrapure water for 20 sec each and the developer working solution (silver stain enhancer and silver stain developer 1:50) added for 2-3 min until protein bands appeared. The developing process was stopped with a 5% acetic acid stop solution. Digital imaging was conducted with the Molecular Imager ChemiDoc™ MP System.

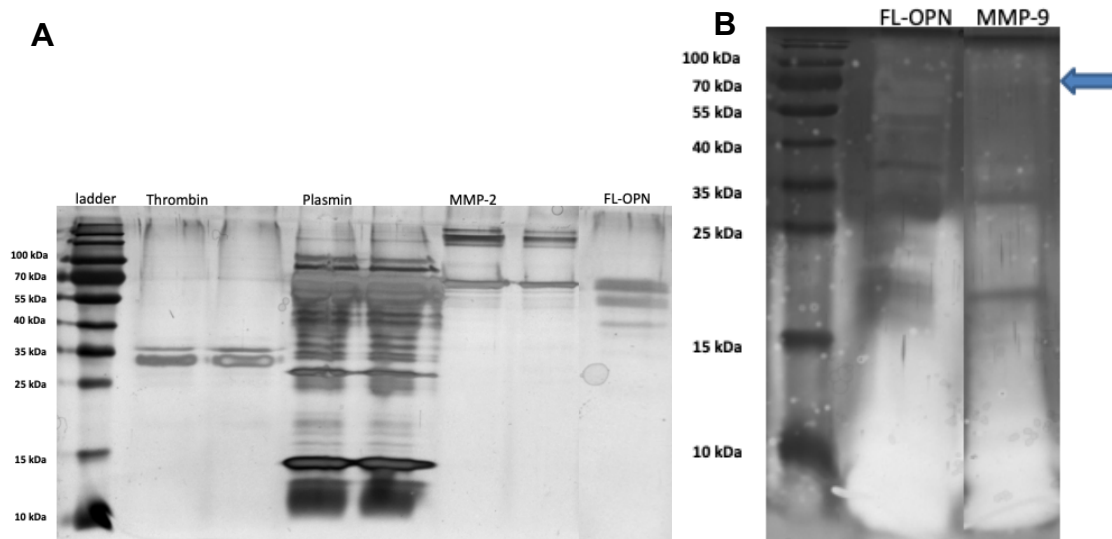


Figure 1: Silver stain of FL-OPN and OPN fragments. To validate that FL-OPN is spliced by enzymes, OPN fragments were detected by silver stain (A, B). The fragments vary in their length. The blue arrow (B) indicates the absence of a visible band in the size of FL-OPN after incubation with MMP-9.

2.2.3 Production of APS

Prior to working with human thrombocytes, our protocol had been approved by the ethics committee of Heinrich-Heine University Düsseldorf (reference number: 2018-248-FmB, 2018-248_1).

2.2.3.1 Isolation of human platelets

Human platelets were isolated from fresh whole blood donor samples. Whole donor blood was centrifuged at 200 x g for 10 min at room temperature with a soft start and soft cessation. By centrifugation a three-phase suspension was formed. To obtain the thrombocytes only the upper phase, which is called 'platelet rich plasma' (PRP), was aspirated carefully and transferred to a 15 ml tube. At a rate of 1:1, 2 ml PBS (pH=6.5), 2.5 U/ml apyrase and 1 µM PGE₁ were added to prevent early coagulation of the thrombocytes before the suspension was centrifuged at 850 x g for 6 min at room temperature. The supernatant was discarded, and the pellet was resuspended in 200 µl Tyrode solution. It is an isotonic solution to protect the cells from dehydration. Total cell count was obtained using the automated hematology analyzer KX-21N. For the following experiments a total number of 70 million platelets were utilized.

Tyrode stock solution (adjust to pH=7.4 with 0.1 % heat inactivated BSA)

	10 x
NaCl	8.01 g
KCl	208.8 mg
NaHCO ₃	1.008 g
NaH ₂ PO ₄	55.2 mg
glucose	0.992 g

Ready-to-use 5 ml 1x Tyrode solution

Distilled water	4500 µl
10 x Tyrode stock solution	500 µl
10 % glucose	49.5 µl
10 % BSA	50 µl
MgCl ₂ (0.1 M)	45 µl

2.2.3.2 Activation of human platelets

Activation with collagen-related peptide (CRP)

Platelets were activated with 5 µg/ml CRP at the rate of 1:10 (10 µl CRP and 90 µl cell suspension). CRP is a synthetic collagen containing repetitive GPO (Glycine, Proline, Hydroxyproline) motifs cross-linked by N- and C-terminal cysteine or lysine residues. This specific structure allows it to be a strong selective GPVI platelet agonist and imitates the cascades of platelet activation during a vascular injury. CRP was incubated for 5 minutes at 37 °C for activation of the thrombocytes.

Activation with adenosine-5'-diphosphate (ADP)

The experiments were also conducted with another thrombocyte agonist, ADP, at the same rate as CRP. The interaction occurs via ADP-receptors on the thrombocyte's surface. Thrombocytes were incubated with a final concentration of 10 µM for 10 min at 37 °C. Following platelet activation utilizing CRP and ADP, 1 U/ml apyrase was added to the suspension and centrifuged at 850 x g for 5 minutes at room temperature. The supernatant was collected and stored at – 20 °C overnight.

2.2.4 Verification of platelet activation

2.2.4.1 Flow cytometry

The activation of platelet was confirmed by flow cytometry which is a method to quantify and identify the expression of cell surface markers of single cells in solution. Enhancing the method with FACS which stands for 'fluorescence activated cell sorting', enables different cell populations to be sorted according to different fluorescent markers.

To briefly describe the method, single cells in solution pass through a flow cell and are exposed to focused laser beam. By means of their light-scattering, cells can be characterized in their volume (=forward scatter/FSC) and granularity (=side scatter/SSC). Fluorescent antibodies which bind to specific antigens on cell surface are activated at specific wavelength which gives an additional information of cell type. Flow cytometry tubes were prepared with the following antibodies to probe the activation status of platelets:

- 1) CD61 antibodies (PE labeled=R-Phycoerythrin) to identify β_3 integrins on inactivated and activated platelets.
- 2) CD62-P antibodies (PE labeled) to identify P-Selectin on activated platelets.
- 3) PAC1 antibodies (FITC labeled=Fluorescein Isothiocyanate) to identify $\alpha_{IIb}\beta_3$ integrins on platelets.

The antibodies were diluted at a ratio of 1:10 before use. Subsequently, 5 $\mu\text{g/ml}$ CRP and 5 μM ADP as well as 50 000/ μl of isolated platelets were added. A sample consisted of 3 μl antibody dilution and 27 μl platelet agonist. The tubes were manually shaken to mix the contents and incubated at room temperature for 15 min in a dark environment to provide optimal conditions for antibody binding resulting in optimal fluorescence. After incubation, the reaction was stopped by adding 400 μl PBS and vortexed before measurement. The samples were vortexed and localized beneath the flow cytometer to be measured and analyzed. The measurement was conducted by the flow cytometer FACSCalibur™ and data analyzed utilizing mean fluorescence intensity (MFI) of the platelet specific population.

2.2.5 Investigation of gene expression

The investigation of the effects of activated platelet supernatants and osteopontin fragments on cellular gene expression level included the following steps.

2.2.5.1 RNA isolation

After transferring the aqueous phase into new tubes, the RNA was isolated utilizing the RNeasy® Mini Kit according to the manufacturer's protocol. In detail, one volume of RLT buffer including 10 μl β -ME/ml was added to the solution and vortexed. One volume of 70% ethanol was added to the lysate to precipitate the RNA for optimal binding to the columns. 700 μl of each sample was transferred to spin columns which were placed in 2 ml collection tubes and centrifuged at 8000 x g for 15 sec at room temperature. The flow-through was discarded and the process repeated with further aliquots of the sample. After discarding the flow-through, 700 μl RW1 buffer was added to the spin column and centrifuged at 8000 x g for 15 sec at room temperature.

The flow-through was discarded and 500 µl of RPE buffer, which had been diluted with 4 volumes of 100 % sterile ethanol before use, was added. Then centrifugation at 8000 x g for 15 sec followed, to wash the spin column membrane. After discarding the flow-through, the process was repeated with a prolonged centrifugation for 2 min. According to the protocol, this step is required to dry the spin membrane so that no residual ethanol is carried over to the RNA elution which might affect the quality of the RNA. RNeasy spin columns were placed in new 2 ml collecting tubes and centrifuged at full speed for 1 min to completely dry the membrane. Thereafter, the spin columns were placed in new 1.5 ml collecting tubes and RNA was eluted by adding 30 µl of RNase-free water and centrifuging at 8000 x g for 1 min.

The final concentration of the RNA was measured by NanoDrop™ spectrophotometer. After initializing the software, blank measurements were performed twice with RNase-free water. 1 µl of RNA eluate was pipetted onto the pedestal, the arm was closed, and the concentration measured by the optical density of the wavelength at 260 nm. The quality of the RNA was calculated by two ratios: $OD_{260nm}/OD_{280nm} \sim 2$
 $OD_{260nm}/OD_{230nm} \sim 2$

2.2.5.2 cDNA synthesis

RNA was processed to cDNA by applying a high-capacity cDNA reverse transcription kit according to the manufacturer's protocol (Applied Biosystems, USA). cDNA was synthesized through complementary base pair formation. In brief, the RNA was diluted with RNase-free water to the minimal available concentration varying between 11.1-25.2 ng/µl. Mastermix per sample was prepared including the following components:

RT buffer	2 µl
dNTP	0.8 µl
Primer	2 µl
RNase inhibitor	1 µl
Reverse transcriptase	1 µl
RNase free water	3.2 µl

10 μ l Mastermix was added to 10 μ l RNA dilution and briefly centrifuged to spin down the content. A C1000 Touch Thermal Cycler (Bio-Rad, USA) was used for reverse transcription:

Step	Temperature	Time	
Step 1	25 °C	10 min	primer binding to the RNA
Step 2	37 °C	120 min	transcription to cDNA
Step 3	85 °C	5 min	denaturation of the reverse transcriptase
	4 °C	∞	

2.2.5.3 Real-time polymerase chain reaction (qPCR)

This method is used to amplify specific DNA sequences in real-time. To compare the gene expression of different genes of interest between different treating groups, qPCR was performed. The fluorescent detection of DNA amplification was achieved by utilizing an intercalating dye (SYBR® Green I) which incorporates into double-stranded DNA and emits fluorescent signals during the exponential amplification phase, leading to a semi-quantitative analysis. The genes of interest included:

human recombinant osteopontin (OPN)

human matrix-metalloproteinase 2 (MMP2)

human matrix-metalloproteinase 9 (MMP9)

human Collagen Type I (COL1A1)

human Collagen Type III (COL3A1)

The final volume of a qPCR sample consisted of 19 μ l Mastermix and 1 μ l of primer of interest which was pipetted into a 96-well plate.

cDNA	1 μ l
SYBR Green I Mix (DNA polymerase, buffer, MgCl ₂ , dNTP, SYBR Green I dye)	10 μ l
RNase free water	8 μ l
Primer	1 μ l

The plate was centrifuged briefly to spin down the content and loaded on a qPCR machine (Bio-Rad CFX 96). The program included the following steps:

Steps	Temperature	Time	
Step 1	50 °C	2 min	
Step 2	95 °C	3 min	denaturation of cDNA
Step 3	95 °C	15 sec	amplification, 45 cycles in total
Step 4	60 °C	1 min	
Step 5	20 °C	5 min	

For the endogenous control of gene regulation, glyceraldehyde-3-phosphate-dehydrogenase (GAPDH) was utilized as a housekeeping gene. A housekeeping gene is known to be not affected by exogenous or endogenous stimulation in its expression so that the expression should be constant. Hence, target genes could be relatively quantitated by comparing their expression to the housekeeping gene.

2.2.6 Investigation of metalloproteinase activity

The effects of APS and various osteopontin fragments were investigated on the protein level. Our work focused on measuring levels of active matrix-metalloproteinases with degradation capability (rather than total enzyme concentration). MMP-2 and -9 are well-known gelatinases. Their activity can be determined through analysis of morphologic degradation of gelatin-based gel using zymography.

2.2.6.1 Bicinchoninic acid protein assay (BCA Protein Assay)

To obtain supernatants without disruptive protein factors, the aforementioned experiments (cf 2.2.3 and 2.2.5) were conducted utilizing serum-free media. Cells were starved in serum-free media for up to 48 h after seeding prior to APS or OPN-fragment exposure. The exposure itself also took place in serum free media.

To investigate the activity of metalloproteinases, the supernatant of each well was collected in separate tubes. Tubes were centrifuged at 300 x g, at 4 °C for 3 min to dispose of cell debris and other cell components. The supernatant was aspirated and transferred to separate tubes for protein measurement. The protein concentration in supernatants was determined using the Pierce™ BCA Protein Assay kit according to the manufacturer's protocol. This assay is based on chemical

reduction of Cu^{2+} to Cu^{1+} in an alkaline medium. The bicinchoninic acid reacts with the reduced cuprous cation causing a color change in the protein solution which can be detected by a spectrophotometer. The BCA-copper complex exhibits a strong linear absorbance at 562 nm with increasing protein concentrations. The general protein concentrations were determined in relation to the standard of a common protein, in this case bovine serum albumin. Briefly, diluted BSA standards were prepared as a reference to protein samples of unknown concentration. Protein samples were measured in replicate. Standard concentrations of 25-2000 $\mu\text{g/ml}$ (plus blank) were utilized. Working reagents were mixed, and 25 μl of each standard or protein sample were added to 200 μl working reagent. The solutions were pipetted into a 96-well plate and incubated for 30 minutes at 37 °C. The samples were measured with a spectrophotometer at 562 nm. A standard curve was plotted and applied to determine the protein concentration of each sample.

2.2.6.2 Gelatin zymography

Gelatin-based gel digestion can be detected as white bands after Coomassie staining (Figure 2). For the production of gelatin-based gel, a modified protocol by Tajhya et al. (80) was used using information from the product data sheet (ABCAM®). The final concentration of acrylamide in our separating gel was 7.5 % and included following components:

component	volume
lower buffer pH 8,8	2.08 ml
30% acrylamide	2 ml
distilled H_2O	2 ml
gelatin (4mg/ml)	2 ml
10% APS	0.08 ml
TEMED	0.01 ml

Stacking gel:

component	volume
upper buffer pH 6,8	1.3 ml
30% acrylamide	0.67 ml

H ₂ O	3.075 ml
10% APS	0.05 ml
TEMED	0.01 ml

As soon as the separating gel was polymerized the overlaying ethanol was decanted and stacking gel poured onto the top. After inserting the well comb, the gel was polymerized for further 20 min and stored at 4 °C overnight to allow the gel to harden. The gel was loaded with an average protein concentration of 20-30 µg of each sample. Each gel contained one positive control of MMP-9 (diluted 1:40) and MMP-2 (diluted 1:10). The electrophoresis started with a pre-phase of 10 min at 120 V which was followed by a running time of 60 min at 120 V until the loading dye reached the bottom of the gel. The gels were then removed from the chamber and incubated in 100 ml of renaturing buffer, containing 2.5 % Triton X solved in distilled H₂O, for 30 min at room temperature with gentle agitation. The renaturing buffer was removed, and the gel was incubated in 100 ml developing buffer (50 mM Tris HCl, 5 mM CaCl₂, 200 mM NaCl, Brij-35 0,02%) in a separate container for 30 min at room temperature with gentle agitation. After the preincubation, gels were washed two times in 100ml distilled H₂O. Subsequently, the developing buffer was replaced, and the gel incubated for development at 37 °C for up to 42 h.

Prior to staining with Coomassie blue staining solution, the gel was washed three times with 100 ml pure water for each 5 min. Coomassie blue staining solution was prepared with 1% Coomassie blue G 250, 10% ethanol (100%) and 5% acetic acid. The incubation for staining took place at room temperature for 1 h. The gel was placed in a container with 100 ml water and the intense color washed out for 48 h prior to digital imaging with Imager (Molecular Imager ChemiDoc™ MP System).

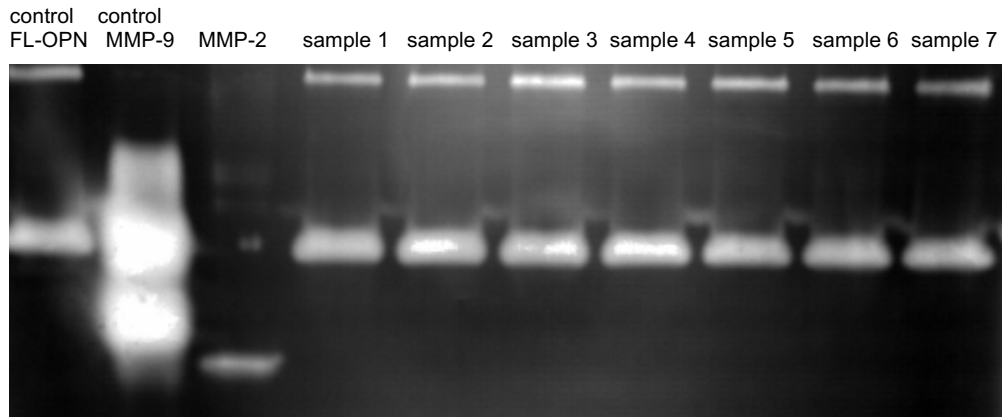


Figure 2: Representative gelatin zymography for detection of MMP-2 and MMP-9 activity in M1-macrophages. MMP-9 activity was assessed in the presence of substrate (OPN, OPN cleaving enzymes). White bands are visible after Coomassie Blue staining. Band intensity was measured and analyzed by Image J.

2.2.7 Statistics

Statistical analysis was performed using GraphPad Prism software version 9.0. The normality of each treatment and control group was tested by Shapiro Wilk test. In case of a positive result, unpaired Student's t-test was performed to compare two different treatment groups. To analyze three different interindividual treatments, one-way ANOVA test was operated. The statistical differences were quantified by Holm-Sidak's post-hoc test. For non-parametric analysis, Mann-Whitney test was performed. P value ≤ 0.05 was considered to be significant.

3. Results

3.1 Stiffness related gene expression in response to APS exposure

3.1.1 M1-macrophages show the strongest OPN response to APS exposure

Comparing the gene expression in the aortic cell types by qPCR, M1-macrophages synthesized the most OPN in response to APS exposure (fold change > 200; Fig 3). Further, OPN gene expression varied between different treatment groups, such that CRP-activated platelet supernatant caused the most, followed by ADP-activated platelet supernatant, and with resting platelet supernatant showing the smallest effects (fold change 256.95 > 228.88 > 207.07).

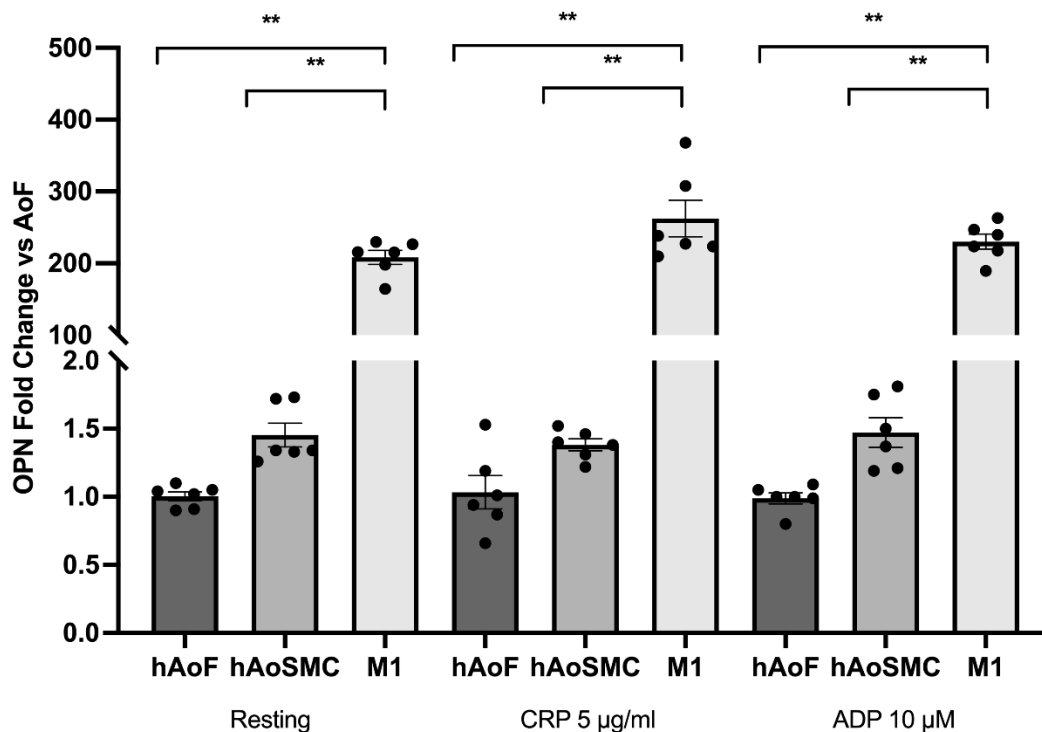


Figure 3: OPN gene expression in response to APS exposure in different aortic cell types. OPN gene expression in hAoSMC and M1-macrophages was normalized to AoF in each treatment group. APS exposure for 6 h caused the strongest OPN gene expression in M1-macrophage, followed by human aortic smooth muscle cells and the least in human aortic fibroblasts. CRP activated supernatant presented the strongest response in OPN gene expression in M1-macrophages. ** p-value < 0.001; one-way ANOVA with Holms-Sidak post-test.

3.1.2 APS downregulates stiffness-related gene expression in hAoSMC and hAoF

When exposed to APS for 6 h, OPN and MMP-2 gene expression are significantly downregulated in hAoSMC and hAoF (Figure 4). Collagen expression is also significantly downregulated, suggesting that fibrosis by these aortic cells is negatively affected by APS exposure (Figure 5).

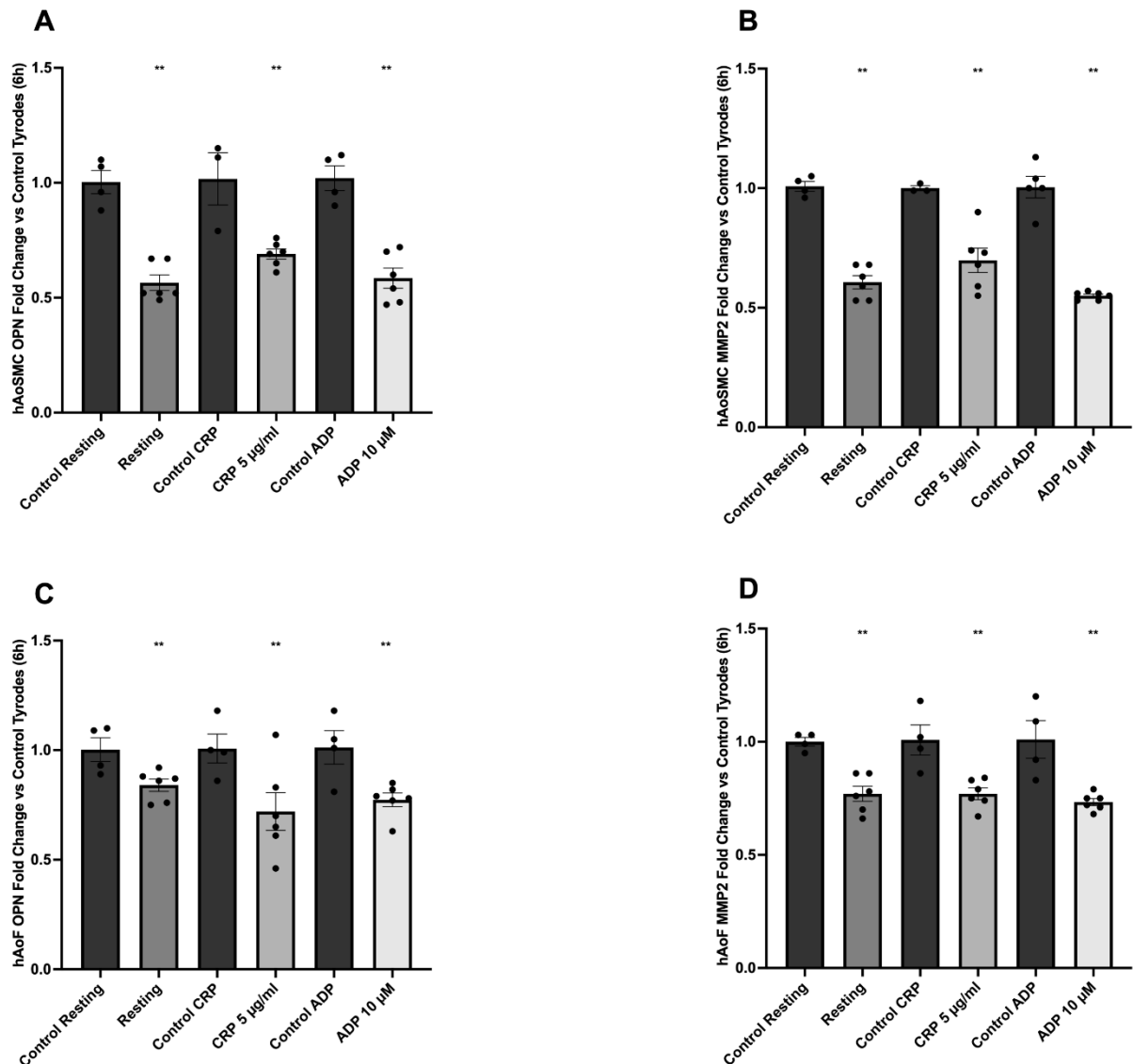


Figure 4: OPN and MMP-2 gene expression in response to APS exposure in aortic resident cells. APS exposure for 6 h significantly downregulated OPN and MMP-2 gene expression in hAoSMC (A, B) and hAoF (C, D) by qPCR. ** p-value < 0.001 vs each Tyrode control; Mann-Whitney Test.

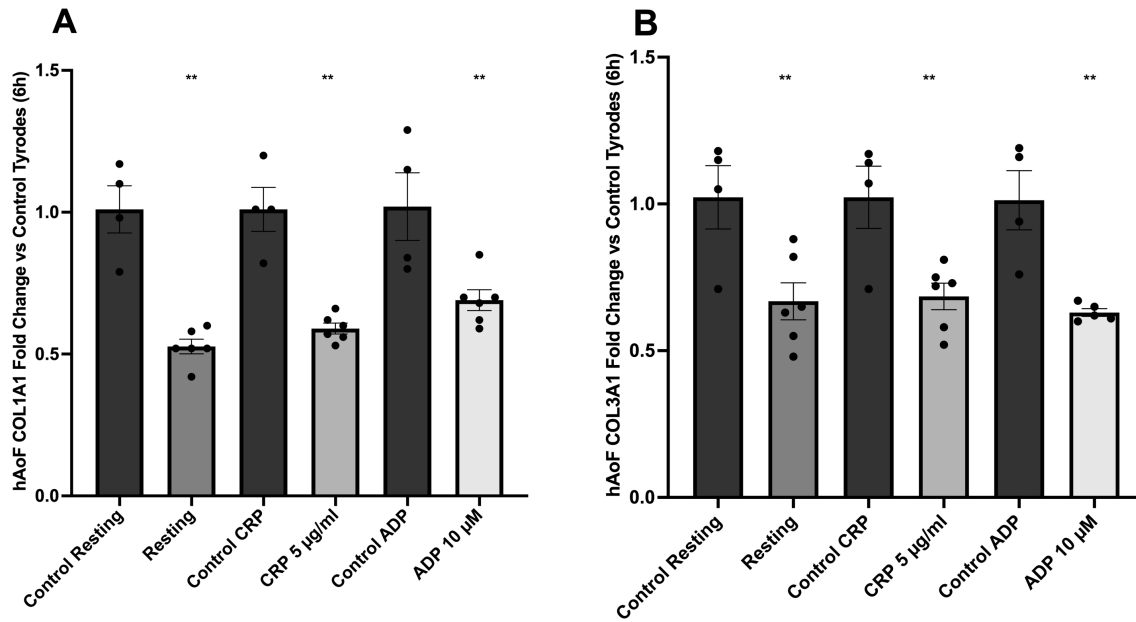


Figure 5: Collagen gene expression in response to APS exposure in hAoF. APS exposure for 6 h significantly downregulated COL1A1 and COL3A1 gene expression in hAoF evaluated by qPCR. ** p-value < 0.001 vs each Tyrode control; Mann-Whitney Test.

3.1.3. APS upregulates OPN and MMP-9 gene expression in M1-macrophages

Short-term APS exposure resulted in increased OPN and MMP-9 gene expression in M1-macrophages. While MMP-9 expression was more up-regulated by ADP-activated platelets, OPN expression was more affected by CRP-activated platelet supernatant (Figure 6 A, B). After 24 hours OPN gene expression, was still significantly upregulated in cells that were incubated with resting platelet supernatant. Compared to the resting platelet group, CRP- activated supernatant presented significantly higher OPN expression. MMP-9 gene expression was significantly downregulated in all three treatment groups (Figure 6 C, D).

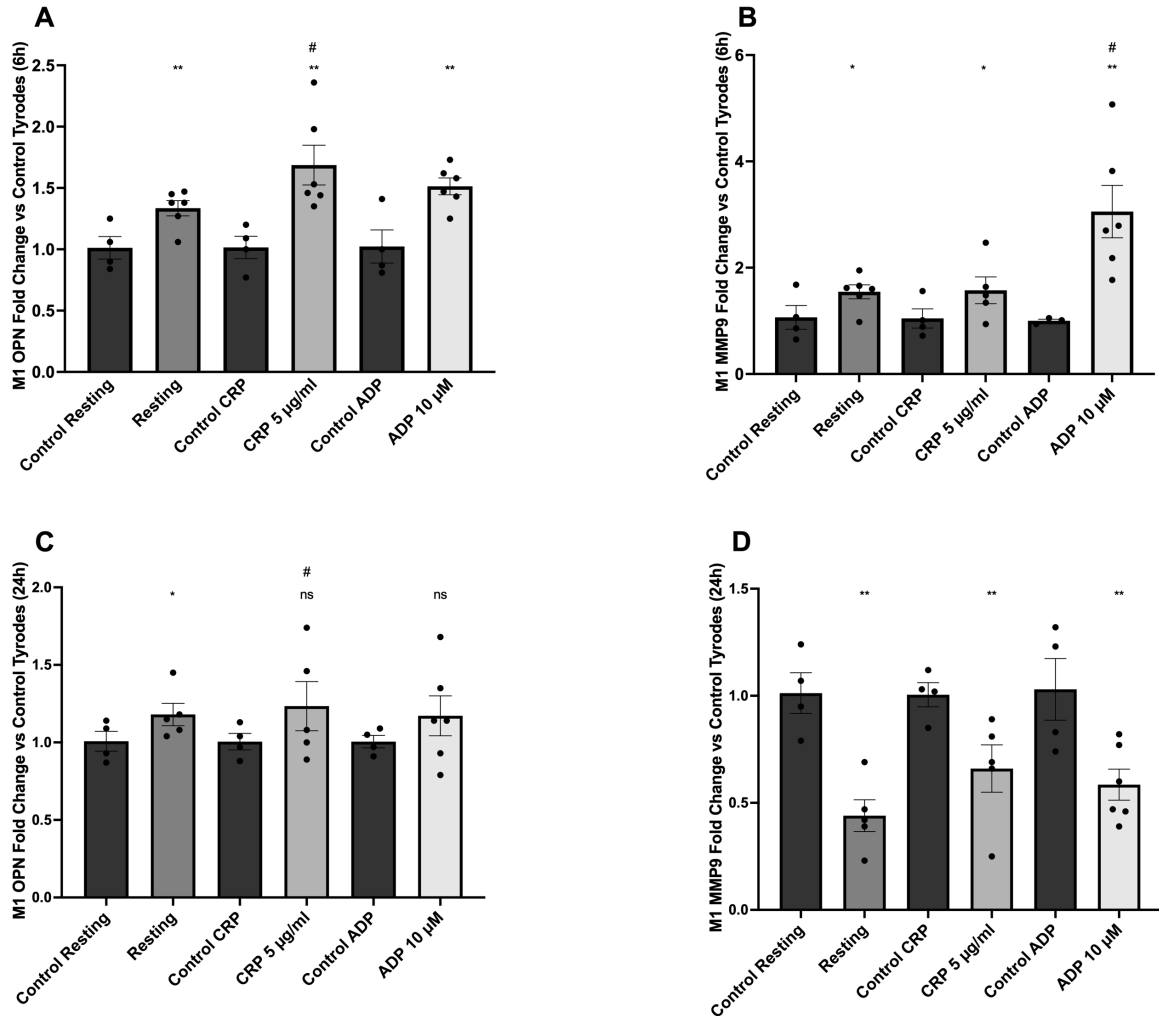


Figure 6: OPN and MMP-9 gene expression in response to APS exposure in M1-macrophages. APS exposure for 6 hours significantly upregulated OPN and MMP-9 gene expression in M1 macrophages (A, B). The strongest effect was seen by CRP activated supernatant for OPN gene expression (A) and ADP activated supernatant for MMP-9 gene expression (B). 24-hour APS incubation presented significant OPN upregulation in resting platelet supernatant group. CRP activated supernatant presented the highest fold change when normalized to resting platelet supernatant (C). MMP-9 was significantly downregulated after 24-hour-exposure to all three different APS (D). ** p-value < 0.001 vs Tyrode controls; Mann-Whitney Test. # p-value < 0.05 vs Resting platelet treated group.

3.2 Effects of APS on MMP-9 activity

3.2.1 APS upregulates MMP-9 activity in M1-macrophages

MMP-9 is commonly found in AAA tissue, and M1-macrophages are known as the main source. Following up on the observed increased gene expression of MMP-9 in M1-macrophages after 6-hour APS exposure, we wanted to explore if APS could directly affect MMP-9 activity by gelatin zymography. Figure 7 shows the statistical

analysis of the band intensity between differently treated M1-macrophages for 6 hours. Compared to Tyrode-only treated cells, APS-treated M1-macrophages showed significantly increased MMP-9 activity. Here, resting platelet supernatant had the strongest effect. When comparing the effects of different supernatants separately, ADP-activated platelet supernatant affected the MMP-9 activity the most, which was concordant with MMP-9 gene expression.

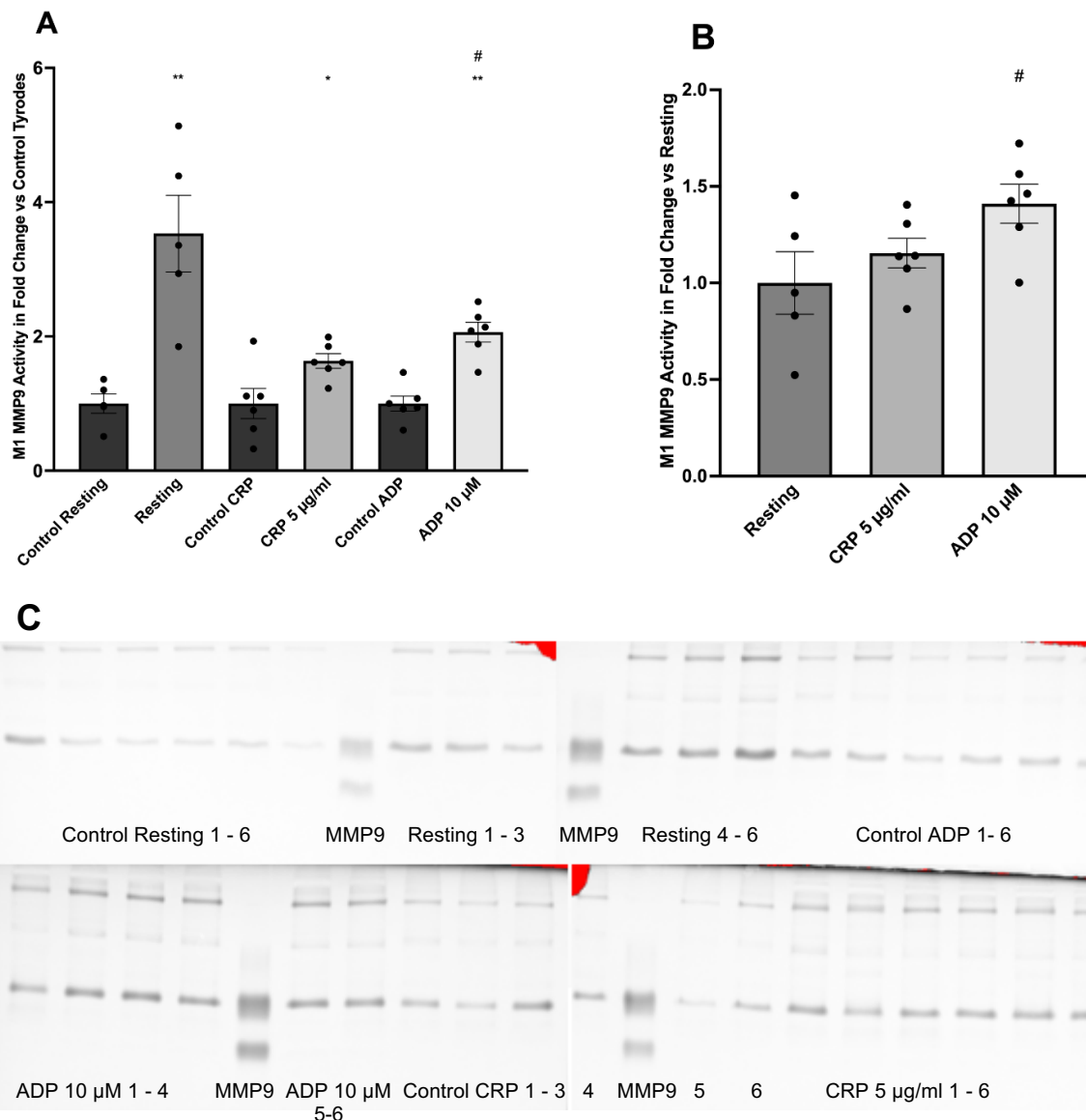


Figure 7: MMP-9 activity in response to APS exposure in M1-macrophages. 6-hour exposure to APS significantly upregulated MMP-9 activity in M1-macrophages observed by gelatin zymography. Resting platelet supernatant resented the highest fold change when compared to each Tyrode controls (A). After normalization to resting platelet supernatant, ADP activated supernatant had the strongest response in MMP-9 activity upregulation (B). (C) shows MMP-9 activity in differently treated M1-macrophages by band intensity of gelatin zymography in 4 different gels. Each gel contains MMP9 control for normalization. ** p-value < 0.001 vs controls; Mann-Whitney Test. # p-value < 0.05 vs resting platelet.

3.3 Stiffness related gene expression in response to OPN treatment

OPN was our gene of major interest and was noted to respond significantly to APS exposure. Thus, we explored the downstream effects of FL-OPN and OPN fragments on the stiffness related gene expression in aortic cells by qPCR.

3.3.1 MMP-2 gene expression is not regulated by OPN fragments in hAoSMC

Literature has shown that FL-OPN upregulates MMP-2 gene expression. We confirmed these results in our experiments. OPN fragments that were generated by thrombin or plasmin did not regulate MMP-2 gene expression significantly after 6- or 24-hour incubation (Figure 8).

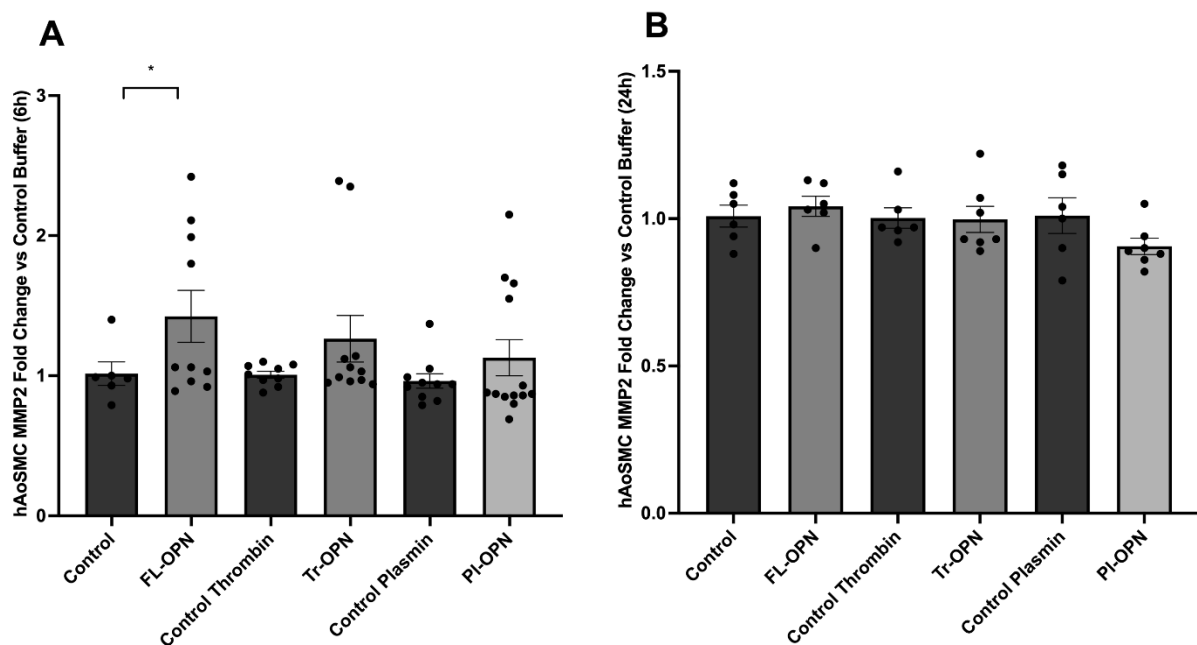


Figure 8: MMP-2 gene expression in response to OPN exposure in hAoSMC. On 6-hour exposure to FL-OPN and OPN fragments, only FL-OPN had significant upregulating effect in MMP-2 gene expression (A). After 24 hours the effect was normalized (B). * p-value < 0.05 vs each control buffer; Mann-Whitney Test.

3.3.2 Stiffness related genes are downregulated by OPN in hAoF

Short-term exposure to FL-OPN and OPN fragments mainly downregulated stiffness-related gene expression in hAoFs, particularly, the thrombin-cleaved OPN fragment (Figure 9 A-C). After 24-hour-exposure, MMP-2 and collagen gene expression trended towards minimal upregulation by FL-OPN, however significant

downregulation of MMP-2 and collagen by OPN fragments was consistent (Figure 9 D-F).

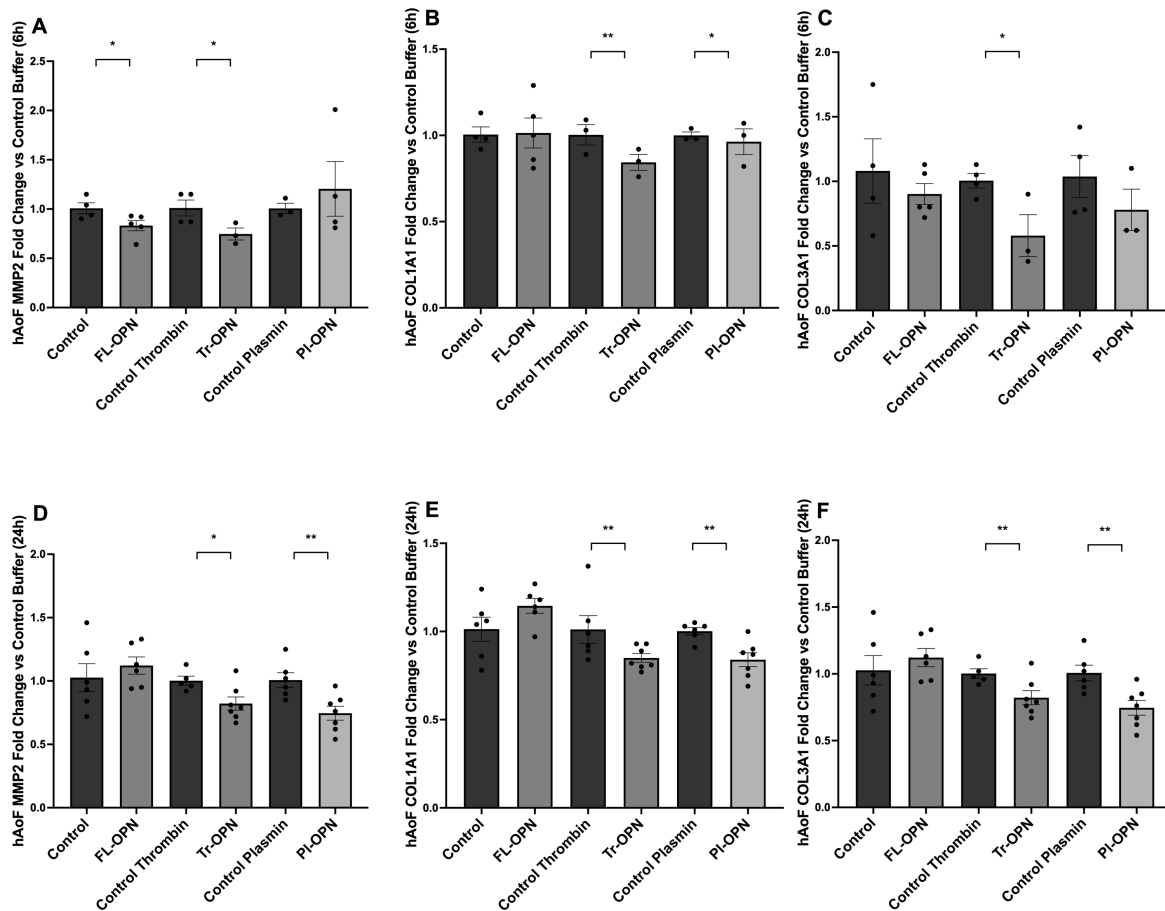


Figure 9: Stiffness related gene expression in response to OPN exposure in hAoF. In hAoF cell culture, both FL-OPN and Tr-OPN significantly downregulated MMP-2 gene expression after 6- and 24-hour-incubation (A, D). Collagen type 1A and 3A gene expression was significantly downregulated by OPN fragments after 6 as well as 24 hours (B, C, E, F). * p-value < 0.05 vs each controls; ** p-value < 0.001 vs each controls. Mann-Whitney Test.

3.3.3 MMP-9 expression is not significantly regulated by OPN in M1-macrophages

MMP-9 was our target gene to explore OPN downstream effects in M1-macrophages. 6-hour-exposure of FL-OPN displayed an upregulating but non-significant trend (Figure 10 A). After 24 hours, thrombin-cleaved OPN fragment led to MMP-9 upregulation that was also non-significant (Figure 10 B).

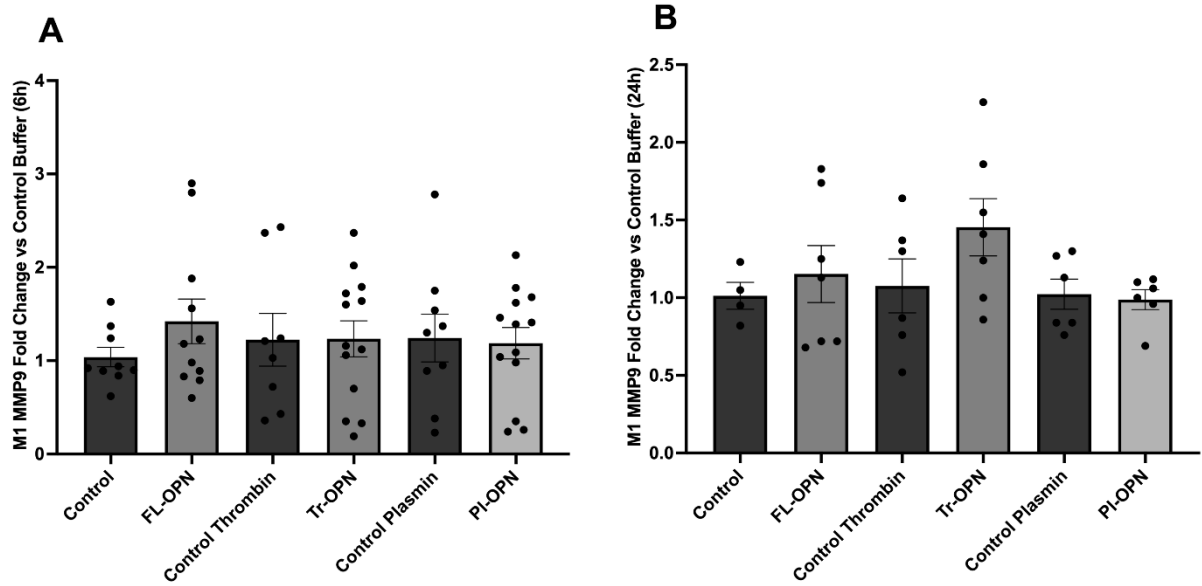


Figure 10: MMP-9 gene expression in response to OPN exposure in M1-macrophages. Both, FL-OPN and OPN fragments did not significantly regulated MMP-9 gene expression in M1-macrophages after 6- and 24-hour exposure when compared to each control buffer group (A, B). Tr-OPN non-significantly upregulated MMP-9 gene expression after 24 hours when compared to thrombin control buffer (B). Mann-Whitney Test.

3.4 Effects of OPN on MMP-9 activity

Similar to APS experiments, we investigated if MMP-9 activity was regulated by OPN and its fragments in M1-macrophages by gelatin zymography.

3.4.1 MMP-9 activity in M1-macrophages appears affected by long-term OPN exposure

24-hour exposure to either FL-OPN and OPN fragments did not regulate MMP-9 activity in M1-macrophages (Figure 11 A, B). However, after 48-hour incubation, Tr-OPN non-significantly upregulated MMP-9 activity compared to thrombin-only exposed cells (Figure 11 C). Compared to FL-OPN, both Tr-OPN and PI-OPN significantly upregulated MMP-9 activity in M1-macrophages (Figure 11 D).

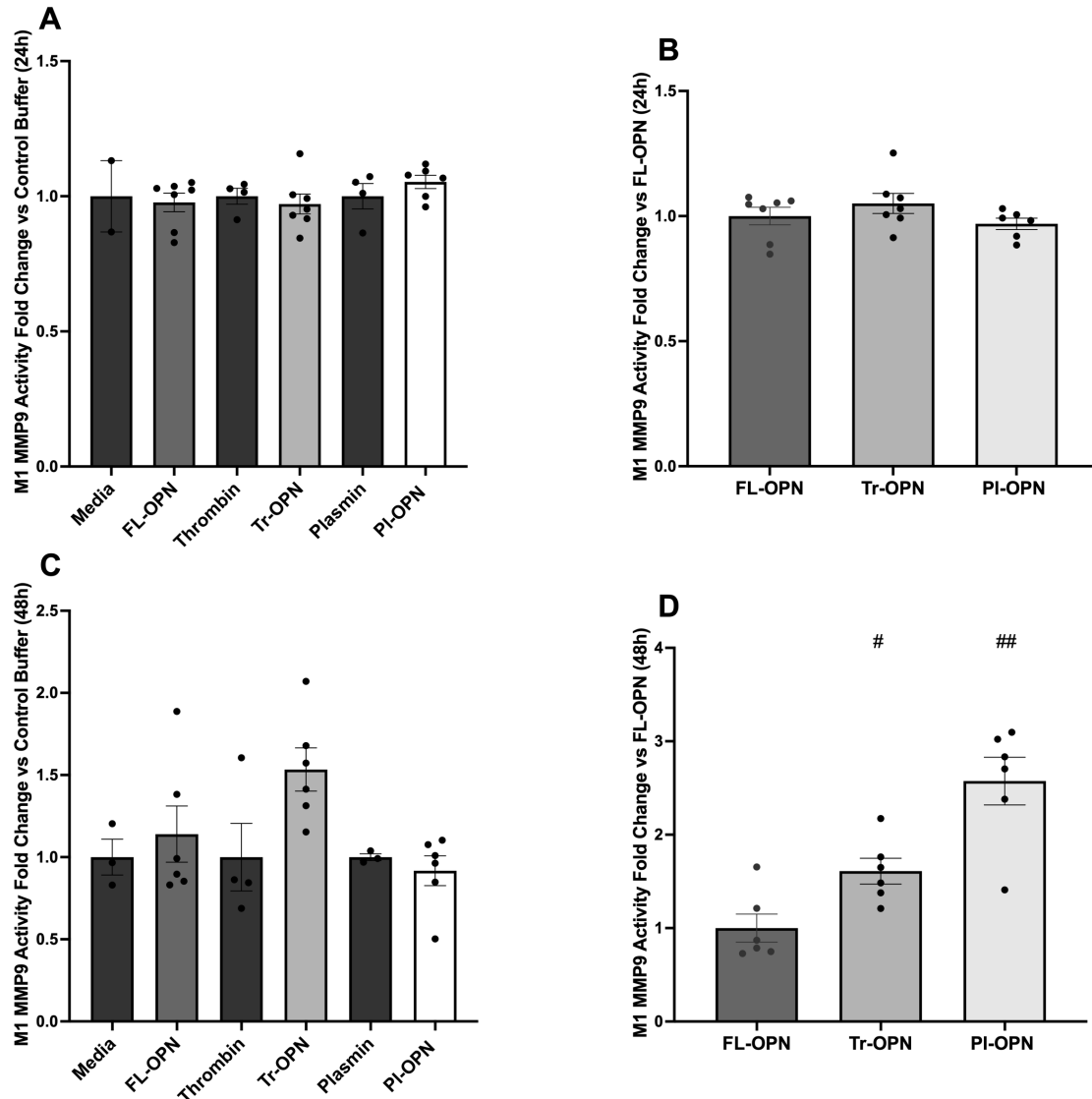


Figure 11: MMP-9 activity in response to long-term OPN exposure in M1-macrophages. Gelatin zymography displayed that 24-hour-exposure to OPN and OPN fragments did not regulate MMP-9 activity in M1-macrophages when compared to both, each control groups and FL-OPN (A, B). After 48 hours, Tr-OPN presented an upregulating trend (C) which was significant when compared to FL-OPN (D). PI-OPN significantly upregulated MMP-9 activity when compared to FL-OPN (D). # p-value <0.05; one-way ANOVA with Holm-Sidak post-test; ## p-value <0.01; one-way ANOVA with Holm-Sidak post-test.

4. Discussion

The onset of sporadic AAA is mostly based on the aging pathology of the infrarenal aorta. One hallmark of an aging aorta is the loss of elasticity and distensibility of the blood vessel, with increasing stiffness. Histological characteristics include enzymatic destruction of elastin lamellae in the media, and deposition of immature, abnormal collagen that lacks cross-linking in the adventitia. The pathologic aneurysmal aortic wall is significantly stiffer, which can be clinically measured by pulse wave velocity, either as a difference between the carotid and femoral, or brachial and ankle pulse waves. However, PWV has a high standard deviation as it depends on patients' blood pressure at the time of measurement. Another measurable factor, which is less dependent on blood pressure, is the cardio-ankle vascular index (CAVI) that relies on the stiffness parameter β , and is obtained by calculation. A multivariate analysis revealed that AAA presence is the only significant statistical parameter that correlated with an enhanced PWV in AAA patients. Interestingly, CAVI remained increased in EVAR patients at 6 months, whereas it decreased in patients with OR. This result raises the question of how remodeling of the non-extinguished aneurysmal sac influences the pressure and blood flow within the aneurysm in the long-term. The long-term consequences are further closely associated with left-ventricular overload and heart failure as increased aortic stiffness enhances myocardial work along with endo- and myocardial oxygen demand in systole, accompanied by decreased myocardial oxygen supply in diastole (81). In fact, only a few studies have raised concerns about the negative long-term effects on left-ventricular dysfunction in EVAR patients (82), (83).

As regards to the involvement of VSMC in arterial stiffness in AAA disease, disrupted mechano-sensation has been reported by Qian et al (84). Pathologic overexpression of α -actinin 2, a protein which is part of the VSMC cytoskeleton, had been explored as a possible cause which would develop gradually over the course of experimental murine AAA. Mitigated intracellular signaling of mechano-sensation enhanced the activity of the Ca^{2+} channel Piezo 1, thereby causing enhanced influx of Ca^{2+} ions and activating cytoskeletal motility in VSMC. In fact, EVAR patients taking Ca^{2+} channel blockers had beneficial outcomes when AAA sac shrinkage was identified

post-intervention.

Age-related arterial stiffness due to vascular aging is further represented by an enhanced systolic wave reflection to the central aorta. Thus, in AAA a higher PWV can be measured but interestingly the enhanced PWV is not diameter related. A possible reason could be decelerated blood flow in the aneurysmal sac, which contributes to the development of ILT. The presence of ILT reduces the actual intraluminal diameter in a large AAA, possibly affecting measured PWV (85).

The natural history of ILT formation encompasses three basic phases: initial changes in platelet activity, formation of insoluble fibrin clot, and finally fibrinolysis. A study by Di Achille et al. investigated the origin of thrombus formation in intact blood vessels (carotid artery, infrarenal aorta and AAA) and explored regional susceptibility based on altered hemodynamic features (86). Defined as 'Thrombus Formation Potential' (TFP), two basic features are necessary: platelets coming from sufficient high flow-induced shear stress have to be presented to a susceptible region (low wall shear stress and high oscillatory wall shear stress) afterwards. In fact, in computed simulation models, low TFP was measured in AAAs that had a calcified neck region causing high wall shear stress and a high shear jet of blood flow when entering the aneurysmal sac, suggesting high wall shear stress as a protective factor from ILT formation. Conversely, when decelerated blood flow into the aneurysmal sac was observed, secondary vortices and prolonged recirculation was established, enabling enough time for platelet activation and communication with activated endothelial cells and favoring ILT formation. Interestingly, low platelet count has been identified in AAA patients. It has been suggested that more platelets are destroyed and aggregated in ILT within the aneurysmal sac (87).

The inflammatory process when platelets are activated is called 'thrombo-inflammation'. It describes various cellular interactions between activated platelets and activated inflammatory cells as well as vascular resident cells that promotes tissue inflammation at the site of vascular injury. In particular, it involves platelet phenotype changes that are characterized by expression/activation or loss of function of different cell surface receptors in a chronic inflammatory state. This phenomenon provides hints about which cell signaling pathways are active in a

disease state and can be diagnostically utilized as a 'dynamic messenger' of cellular function that indicates hallmarks of the specific disease (88). During inflammatory processes, activated platelets also have an impact on 'immunothrombosis' (89). In the process of plasma coagulation two types of platelets can be identified: 1. procoagulant platelets, which support thrombin and fibrin generation triggered by tissue factor (TF) expression and secretion of TF-positive microvesicles, and 2. aggregating platelets that initiate first clot formation and contraction by binding fibrin via $\alpha\text{IIb}\beta\text{3}$ receptors. They are responsible for the actual thrombus growth progression through the receptor GPVI which binds further fibrin molecules. This cascade eventually results in increased platelet-neutrophil interaction and activation that drives 'immunothrombosis'.

Lastly, atherosclerosis, a risk factor for AAA, also contributes to a regionally stiffened aorta due to plaque deposition in the aortic lumen. Monocytes and platelets are involved as key players. Triggered by oxidized LDL (oxLDL) or podoplanin evolved from inflammatory macrophages, Th17 T cell and fibroblast platelet-activating factor receptor (PAFR) is activated. This reaction can be exaggerated by simultaneous activation of platelets by ADP and thrombin, initiating prothrombotic responses by adhering platelets to the endothelium and recruiting leukocytes (90).

Considering the aforementioned aspects of the stiffening process of the aorta, for our experiments we utilized APS as a possible agent to explore functions of activated platelets in AAA disease. Further, OPN was chosen as the target gene of interest since it was considered as a pro-inflammatory cytokine and a marker gene of synthetic type of VSMC. We discuss our results in detail below.

4.1 Effects of ILT and role of inflammation

ILT volume is associated with faster AAA growth (0.5 mm/y higher growth rate) and an increased risk of rupture (34), (91), (92). Inhibiting thrombus formation has been suggested to limit AAA growth (93).

At sites of vascular injury, platelets adhere to the endothelial matrix and are activated by cellular contact. A decrease in blood flow velocity enhances thrombus formation and aids in restoration of vascular wall integrity. Cellular communication between

platelets and the surrounding cells is achieved via membrane receptors and soluble factors which are released from granules. There are three reported types of platelet granules: α -granules, δ -granules, and lysosomes (which contain proteinases and cytokines). Activated platelets release numerous mediators such as CD40, platelet factor 4 (PF4/CXCL4), and RANTES (CCL5) at the injury site that enhance leukocyte adhesion and promote neutrophil and macrophage recruitment, which is crucial for enhanced tissue inflammation (94), (95), (96). Pro-inflammatory cells, such as M1-macrophages and lymphocytes, are recruited locally to sites of injury after activation via toll-like receptors (TLR) (90).

The accumulation of these various inflammatory processes that are involved in the formation of ILT contribute to AAA progression (94). Chemokine activity is modulated through heterodimer formation (e.g. PF4 and RANTES). Simultaneously, activated endothelial cells secrete van-Willebrand factor (vWF) that interact with platelet receptor (GP1b) which is further linked to interactions with neutrophil β 2 integrins.

In this study we showed that M1-macrophages, as non-resident pro-inflammatory cells, reacted the most to short-term (6 h) APS exposure through significantly upregulated OPN- and MMP-9 gene expression. Interestingly, OPN gene expression was the highest with CRP-activated supernatant, suggesting that CRP is the most potent *in vitro* platelet activator. Our finding that resting platelet supernatant also upregulated OPN gene expression suggests that not only degranulation of activated platelets, but also cell-to-cell interaction plays an important role in vascular pro-inflammatory gene transcription signaling. In fact, ILT is considered to be a location of high biological activity, as it contains multiple active enzymes and cell types that contribute to chronic inflammation.

Sustained upregulation of OPN gene expression after 24 h exposure to APS reflects on-going counter-regulation and biological effects on the cellular level, implying that AAA development requires consistent exposure to pro-inflammatory milieu that generates chronic lingering tissue inflammation.

4.2 Effects of ILT on ECM alteration

Our concordant results of both MMP-9 gene expression and activity being

upregulated the most with ADP-activated platelet supernatant in M1-macrophages, supports that there is a positive correlation between MMP-9 expression and the ratio of thrombus, as has been previously described by Li et al (97). They suggested that increased protease activity (MMP-9) contributes to complement-coagulation crosstalk in the aneurysm wall, leading to increased thrombus formation in AAA lumen. Also, increased MMP-9 activity leads to enhanced degradation of elastin in the aortic wall, decreasing the elasticity of the aorta, and its ability to withstand high-pressure blood flow.

Of note, our experiments showed consistent downregulation of stiffness-related genes in hAoSMC and hAoF cell culture in response to APS exposure, suggesting no in vitro correlation between aortic fibrosis and aortic stiffening via platelet activation. However, few studies have reported on a correlation between the presence of ILT and collagen and elastin turnover, respectively (98). In vivo experiments that utilized porcine pancreatic elastase (PPE) and β -aminopropionitrile (BAPN) for induction of experimental AAA in mice revealed that ILT-containing AAA showed increased wall thickness, and less undulated and more stretched collagen. With increasing volume of ILT, the primary orientation of collagen fibers alters into rectilinear configuration, reducing undulation. Change of collagen orientation results in decrease in biaxial wall stretch. This study also described high deposition of non-crossed collagen but lacking cross-linking, resulting in frustrated inhibition of rapid compensatory deposition to arrest dilatation. They conclude that it is the rate and effectiveness of fibrillar collagen remodeling that dictates aneurysm progression. Further, the same study revealed excessive accumulation of glycosaminoglycans (GAG) and proteoglycans (PG) in aneurysmal tissue. This phenomenon disturbs proper mechanosensing and drives positive feedback for phenotypic change and cell death, which worsens local cellular mechano-reception. Accumulation of GAGs and PGs in the intra-lamellar medial space further disrupts intra-lamellar connection between VSMC and elastic laminae, supporting disturbed cell biology and fragmentation of elastin.

Additionally, a direct interaction between activated platelets and collagen fibrils via the platelet receptor GPVI and vWF has been described by Jones et al (99). By

utilizing collagen-hybridizing peptides that recognize degraded collagen in the aortic wall, the researchers found increased abnormal collagen fibrils in AAA tissue when performing multiphoton imaging. By second harmonic generation microscopy and immunofluorescence they could identify heterogenic platelet adhesion regions. They visualized platelets adhering to intact collagen fibrils only, whereas in regions with increased abnormal collagen fibrils (such as in AAA tissue) platelet adhesion was mostly absent, and the interaction was missing. This phenomenon may explain the heterogeneous reactivity of coagulation in patients. Consequently, they suggested that insertion of collagen-impregnated stent grafts might be protective against post-surgical blood loss in patients.

Less platelet interaction with collagen may also explain ILT development in the course of AAA disease, where platelets are trapped during clot formation but then fail to interact with surrounding collagen matrix.

4.3 Effects of ILT and role of hypoxia

Since ILT causes a chronic hypoxic environment in the aneurysmal sac, effects of hypoxia are briefly covered in this paragraph although no specific experiments were conducted within the frame of the current work to investigate this issue.

The aortic wall covered by ILT is consistently exposed to hypoxia, with decreased mural oxygen partial pressure (100) which correlates with ILT thickness (78). It decreases the oxygen flow by unilateral prolongation of diffusion distance between the luminal blood stream and the underlying tissue (101). Subsequently, synthesis of important aortic wall components such as elastin and collagen by the aortic resident cells is impaired, which might support the growth of aneurysm (100).

Regarding cell proliferation and apoptosis, hypoxia can lead to multiple issues. It can enhance hAoSMC apoptosis, and increase secretion of MMP-2, resulting in enhanced elastin degradation with subsequent aortic wall weakening (78). However, hypoxia can also encourage cell proliferation and migration in the vascular wall mediated by 15-hydroxyeicosatetraenoic acid and upregulated MMP-2 and -9, causing increased overall MMP-9 expression in VSMC (102), (103). In either case, hypoxia has a degrading impact on ECM. Further, within the inflammatory

environment active proteases are covalently bound to neutrophil-gelatinase-associated lipocalin (NGAL), preventing early degradation of these enzymes. Consequently, those enzymes are kept in active form for a prolonged period, which supports elastin degradation (23). Proteolytic enzymes are also reported to cause fissures in the ILT that augment the mechanical stress in the underlying wall, increasing the risk of AAA rupture in hypoxia-weakened AAA wall (104). Finally, hypoxia-induced neovascularization serves as an attractive route for inflammatory cells to the site of the underlying vessel wall below the ILT. Macrophages present higher bioreactivity in a hypoxic environment and increase production of elastases (100).

Having understood the vital role of activated platelets in the process of tissue inflammation and their subsequent effects on ECM alteration, we wanted to explore the downstream effects of the pro-inflammatory cytokine OPN. Does enhanced induction of OPN expression by activated platelets upregulate pro-inflammatory processes within the aneurysmal sac and worsen aneurysmal disease?

OPN and thrombin, an enzyme that is mostly derived from activated platelets, have been reported to coexist wherever blood coagulation is activated due to inflammation (105). Having identified pro-inflammatory M1-macrophages as the main source of the cytokine OPN, we will discuss in the following sections how the induced OPN signaling pathway contributes to aortic stiffening and plays a role in the development of AAA disease.

4.4 Effects of OPN on aortic stiffness: Alteration of ECM by MMP-2, -9

OPN is known to be involved in many different inflammatory processes by increasing macrophage and T-cell activation that promotes calcification in arteries and contributes to arterial stiffening (106), (107), (108),(109). As a result, OPN plasma level is significantly associated with the presence of cardiovascular diseases. In particular, this cytokine is highly expressed in inflammatory cells, particularly M1-macrophages as shown in this work, and can cause arterial restenosis. As a potent macrophage chemotactic stimulus, it regulates macrophage infiltration during the

inflammatory response. More importantly, by concomitant production of IL-12 and CD3, it can exacerbate the chronic inflammatory response which is found in AAA (110).

In AAA disease, increased OPN serum concentration correlates with presence and growth of AAA in large screening studies by affecting the dynamic metabolism of ECM components (21). Moxifloxacin has been shown to induce experimental AAA in a murine model by elevating OPN levels, promoting VSMC phenotype switching to the synthetic type and increasing MMP-2 activity (111).

Several studies have already shown the interplay between FL-OPN and cleaving enzymes (112), (113), (114), (115), but the effects of OPN fragments have not yet been investigated in depth. The C-terminal sequence of Tr-OPN can interact with macrophages via CD44 resulting in macrophage activation, induction of cytokines and MMP secretion. In this way, Tr-OPN contributes to tissue inflammation neutrophil-independently (105). Since thrombin, plasmin and OPN are commonly found at sites of inflammation *in vivo*, we wanted to explore *in vitro* if abundant presence of substrate and enzyme might lead to an environment with the potential to enhance aortic stiffness with their generated products (88).

In this study, we replicated FL-OPN's upregulating effect on MMP-2 gene expression in hAoSMCs (116). MMP-2, or gelatinase A, is constitutively synthesized by hAoSMC and is known as the elastase which contributes the most to early aneurysmal dilatation of the aorta (117), (118). A change of ECM composition resulting from altered ECM remodeling enzyme activity can affect vascular cells' phenotype due to generation of pro-inflammatory microenvironment. VSMCs are known to change from a mature contractile phenotype to an immature proliferative/synthetic phenotype in an inflammatory environment. During vascular remodeling of the ECM, VSMCs are separated from the extracellular matrix which activates phenotypic switching. Further, matrix separation enables infiltration of pro-inflammatory cells into the ECM. Hence, OPN could contribute to the progression of AAA through both ECM alteration and its effects on vascular cell phenotype change, in addition to its role as a pro-inflammatory cytokine (102).

However, in our experiments with thrombin and plasmin cleaved OPN fragments,

no significant upregulating effect was observed either during short- (6 h) or long-term (24 h) exposure in hAoSMCs. In hAoF, MMP-2 gene expression was even downregulated with OPN fragments. Current literature reports about upregulated OPN expression in aortic fibroblasts by fibroblast growth factors or angiotensin II which are enhanced in cardiovascular diseases. To our knowledge, however, downstream effects of OPN or OPN fragments on MMP expression or activity in aortic fibroblasts are not explored yet. Our results are from three independent experiments, so that further investigations with different dosing and time of exposure may be required to gain more insight into molecular effects of OPN in aortic adventitial cells.

M1-macrophages, as non-aortic resident cells, were investigated for their MMP-9 expression and activity in response to OPN exposure. Studies have shown that OPN can be a substrate for MMPs and there is a connected signaling pathway between OPN and MMP-9 activity regulation (119), (120), (121). However, in our experiments MMP-9 gene expression was not significantly upregulated by FL-OPN or OPN fragments during short- or long-term stimulation. Although pro-MMP-9 activity was upregulated after 24-hour-exposure to FL-OPN (data not shown), MMP-9 activity was not regulated. After 48 hours we could see a trend toward upregulating MMP-9 activity by FL- and Tr-OPN but not significantly. With further statistical analysis we showed that Tr- and PI-OPN had a significant upregulating effect on MMP-9 activity in M1-macrophages. This result suggests that OPN-cleaving enzymes like thrombin and plasmin themselves have a powerful ability to regulate MMP-9 activity, which warrants future investigation. The role of MMP-9 is pivotal in that beyond its role in elastin degradation it also functions as potent inhibitor of VSMC contraction, contributing to the initial development of AAA (102).

Interestingly, the activity of MMP-2 and MMP-9 in AAA disease can be further modulated via the ADAR1 pathway (122). In general, MMP function is modulated at different levels, post-transcriptionally or post-translationally. RNA editing is a post-transcriptional modification of MMP's functionality. ADAR1 is known to be involved in mRNA splicing. By physical interaction with human antigen R (HuR) in VSMC, ADAR1 contributes to HuR's stabilization of MMP-2 and MMP-9 mRNA, hence

promoting AAA development.

Notably, MMPs contribute to VSMC calcification, causing subsequent vascular calcified lesions which are common in atherosclerotic disease (102). OPN can act as a calcification inhibitor under physiological conditions (123), as opposed to its role in upregulating MMPs when overexpressed in pathologic conditions such as AAA. Overexpressed MMPs enhance vascular calcification, a process especially notable in advanced age (123), (124).

4.5 Effects of OPN on aortic stiffness: Collagen

Collagen type I and type III make up 80-90% of the total collagen in the aorta (125). Aortic dilatation is commonly accompanied by increased compensatory adventitial thickening. OPN had been previously reported to participate in collagen synthesis during vascular remodeling (126), so we investigated whether collagen synthesis was affected by OPN in our experimental setting.

In our experiments, COL1A1 and COL3A1 gene expression was somewhat but non-significantly increased by 24-hour stimulation with FL-OPN in hAoF. However, Tr- and PI-OPN significantly downregulated both collagen types after 6- as well as 24-hour exposure. Our data did not support the idea that OPN plays a role in aortic fibrosis by upregulating collagen gene expression during aneurysm formation. On the other hand, it had been reported that immature collagen is more soluble than normal aortic collagen and more susceptible to degradation by MMPs. Decreased collagen content and poor cross-linking of collagen fibrils contribute to wall weakness that may also lead to aneurysm formation (117), (127).

Considering the biomechanics, the interaction between elastin and collagen fibers for mechano-sensing and regulation is essential to maintain aortic function. Increased circumferential material stiffness has been reported in aneurysm tissue, which correlates well with the size of aortic lumen enlargement. These phenomena have been explained by increased absence of elastin and subsequent loss of elastic energy storage in the aortic wall that was linked to collagen undulation and altered orientation of collagen fibers in diseased aortic tissue. In fact, it has been reported that straight-oriented collagen fibers stiffen the vessel wall dramatically (128). As

advanced age is a risk factor for AAA, there is likely a gradual microstructural reorganization of collagen and fiber density as well as orientation changes of the intramural cells (such as aortic smooth muscle cells) that affects the circumferential and axial stress in the aortic wall and contributes to aneurysm disease development (129). It may be interesting to investigate if OPN enhances aortic wall stiffness by altering collagen fiber orientation instead of upregulating collagen synthesis.

4.6 Limitations

This work has several limitations. In the framework of this project, we were unable to demonstrate MMP-2 and -9 activity in aortic resident cells (hAoSMC and hAoF). A possible reason could be the lack of sensitivity of the method (gelatin zymography), particularly for MMP-9, as the expression in both cell types was minor (Ct values by qPCR between 34-35).

Also, no experiments under hypoxic conditions were conducted in order not to overly expand the scope of this work. Future studies under hypoxic condition may display more compelling effects of OPN, OPN fragments, and APS in *in vivo* processes.

We utilized primary human aortic cells in culture. However, the behavior of hAoSMC and hAoF may vary depending on their anatomic origin (between abdominal and thoracic aorta). Further, our experimental setting did not completely imitate the *in vivo* inflammatory milieu found within AAA tissue, so that our results may represent only a limited range of *in vivo* pathological signaling events.

As regards the hAoSMC contribution to aortic wall stiffness, investigation of elastin gene or protein expression would have been interesting to evaluate the elastin porosity in the aortic medial layer. The turnover of elastin and collagen content in the aortic wall play an important role for wall stability. Also, elastin porosity may increase hAoSMC apoptosis through loss of cell-matrix connection (129).

Additionally, it has been found in chronic obstructive pulmonary disease (COPD) that elastin fragments may promote naïve M0-macrophage polarization towards pro-inflammatory M1 that are sensitized to elastin-rich tissue. In fact, inhibition of these M1-macrophages decreased AAA progression in a murine model (130). Therefore,

further investigation of fragmented elastin in AAA disease in the context of ILT derived MMPs would be promising in development of new therapeutic strategies.

4.7 Conclusion

Untreated AAA is a life-threatening disease. To-date there is no pharmaceutical treatment to slow down or prevent AAA progression, so that close monitoring is essential. AAAs with ILT are larger and more prone to earlier rupture relative to non-ILT AAA (38),(93). For longitudinal and predictive monitoring, many biological markers have been discussed, including OPN (131). However as of yet, due to a lack of assay sensitivity, it has not been able to be established as a monitoring feature. A pharmacokinetic study assessed the feasibility of utilizing anti-OPN antibody to neutralize its pathological effects with human blood samples. However, due to its remarkably fast turnover (reported half-time of 11 minutes) and fast pharmacokinetics, the administration of conventional antibodies for this purpose seems to be very challenging (132).

This work tried to understand the association of activated platelets in ILT and their effects on OPN signaling and relation to aortic stiffness, which is a pathological feature of AAA development. Degradation of activated platelets upregulated OPN gene-expression in pro-inflammatory M1-macrophages that are known to pathologically enhance inflammation in AAA tissue by recruiting more inflammatory cells and secreting pro-inflammatory cytokines (106). As regards aortic wall damage, MMP-9 gene expression and activity were upregulated, contributing to enhanced elastin breakdown and aortic wall stiffness due to loss of elasticity. Hence, our results suggest that ILT serves as a source of active inflammation by providing OPN as a pro-inflammatory cytokine and ECM degrading molecule, contributing to the pathology of AAA disease.

In our study, FL-OPN in hAoSMC upregulated MMP-2 gene expression, known to contribute to elastin degradation in the medial layer of the aortic wall and limit the elastic compensation of pulsatile blood flow in the aortic lumen. Despite of no upregulating effect on cellular collagen production by OPN exposure in our experiments, decreased collagen synthesis by hAoF may affect mechanical stability of the aortic wall and could result in aneurysm formation. Constant OPN stimuli to M1-macrophages may upregulate MMP-9 activity, adding to elastin malfunction,

elastin loss, and decreased elastin-collagen interactions, further enhancing aortic wall stiffness.

In conclusion, this work identified some correlations between activated platelets in ILT and upregulated OPN and MMP-9 expression, that might contribute to aortic stiffness. Upregulation of MMP-2 and MMP-9 by FL-OPN were observed in hAoSMC and M1-macrophages, a process known to contribute to aortic stiffness. However, fibrosis was not directly regulated by OPN signaling in hAoF. Rather, downregulation of collagen synthesis was observed in this study which is also a hallmark of AAA formation. With the development of more advanced scientific techniques such as single-cell RNA sequencing and multi-photon-based imaging tools, more precise investigations of disease pathway analysis on cellular level have become possible. Further investigation in *in vivo* models and *in vitro* experiments will need to be performed to gain clearer insights into the complex pathology of AAA disease, and to develop strategic treatment plans for future AAA patients.

5. Bibliography

1. Amalinei C et.al, Etiology and Pathogenesis of AA. Intech. 2016.
2. Müller M. Chirurgie für Studium und Praxis. 12th ed. Medizinische Verlags-und Informationsdienste, Breisach; 2013.
3. Kent KC.Clinical practice. Abdominal Aortic Aneurysms. N Engl J Med. 2014.
4. Benson RA et al. Screening results from a large United Kingdom abdominal aortic aneurysm screening center in the context of optimizing United Kingdom National Abdominal Aortic Aneurysm Screening Programme protocols. J Vasc Surg. 2016.
5. Anjum A et al. Is the incidence of abdominal aortic aneurysm declining in the 21st century? Mortality and hospital admissions for England & Wales and Scotland. Eur J Vasc Endovasc Surg. 2012.
6. Khashram M et al. Prevalence of abdominal aortic aneurysm (AAA) in a population undergoing computed tomography colonography in Canterbury, New Zealand. Eur J Vasc Endovasc Surg. 2015.
7. Majeed K et al. Prevalence of abdominal aortic aneurysm in patients referred for transthoracic echocardiography. Intern Med J. 2015.
8. Oliver-Williams C et al. Lessons learned about prevalence and growth rates of abdominal aortic aneurysms from a 25-year ultrasound population screening programme. Br J Surg. 2018.
9. Golledge J. Abdominal aortic aneurysm: update on pathogenesis and medical treatments. Nat Rev Cardiol. 2019.
10. Thompson A et al. An analysis of drug modulation of abdominal aortic aneurysm growth through 25 years of surveillance. J Vasc Surg. 2010.
11. Jacomelli J et al. Editor's Choice – Inequalities in abdominal aortic aneurysm screening in England: Effects of social deprivation and ethnicity. Eur J Vasc Endovasc Surg. 2017.
12. Kuivaniemi H et al. Understanding the pathogenesis of abdominal aortic aneurysms. Expert Rev Cardiovasc Ther. 2015.
13. Sidawy AN. Rutherford's Vascular Surgery and Endovascular Therapy. 9th ed. Elsevier Inc.; 2018.
14. Debus E et al. S3-Leitlinie zu Screening, Diagnostik, Therapie und Nachsorge des Bauchortenaneurysmas.

15. Schmitz-Rixen T et al. Ruptured abdominal aortic aneurysm—epidemiology, predisposing factors, and biology. *Langenbecks Arch Surg*. 2016.
16. Karthikesalingam A et al. Mortality from ruptured abdominal aortic aneurysms: Clinical lessons from a comparison of outcomes in England and the USA. *Lancet*. 2014.
17. Landenhed M et al. Risk profiles for aortic dissection and ruptured or surgically treated aneurysms: A prospective cohort study. *J Am Heart Assoc*. 2015.
18. Sweeting MJ et al. Meta-analysis of individual patient data to examine factors affecting growth and rupture of small abdominal aortic aneurysms. *Br J Surg*. 2012.
19. Makrygiannis G et al. Sex differences in abdominal aortic aneurysm: The role of sex hormones. *Ann Vasc Surg*. 2014.
20. Lederle FA et al. Rupture rate of large abdominal aortic aneurysms in patients refusing or unfit for elective repair. *JAMA*. 2002.
21. Kadoglou NPE et al. Arterial stiffness and novel biomarkers in patients with abdominal aortic aneurysms. *Regul Pept*. 2012.
22. Raaz U et al. Segmental aortic stiffening contributes to experimental abdominal aortic aneurysm development. *Circulation*. 2015.
23. Khan JA et al. Intraluminal thrombus has a selective influence on matrix metalloproteinases and their inhibitors (tissue inhibitors of matrix metalloproteinases) in the wall of abdominal aortic aneurysms. *Ann Vasc Surg*. 2012.
24. Swedenborg J et al. The intraluminal thrombus as a source of proteolytic activity. *Ann N Y Acad Sci*. 2006.
25. Folkesson M et al. Protease activity in the multi-layered intra-luminal thrombus of abdominal aortic aneurysms. *Atherosclerosis*. 2011.
26. Piechota-Polanczyk A et al. The abdominal aortic aneurysm and intraluminal thrombus: current concepts of development and treatment. *Front Cardiovasc Med*. 2015.
27. Fontaine V et al. Involvement of the mural thrombus as a site of protease release and activation in human aortic aneurysms. *Am J Pathol*. 2002.
28. Adolph R et al. Cellular content and permeability of intraluminal thrombus in abdominal aortic aneurysm. *J Vasc Surg*. 1997.

29. Coutard M et al. Thrombus versus wall biological activities in experimental aortic aneurysms. *J Vasc Res.* 2010.
30. Parr A et al. Thrombus volume is associated with cardiovascular events and aneurysm growth in patients who have AAA. *J Vasc Surg* 2012.
31. Kazi M et al. Influence of intraluminal thrombus on structural and cellular composition of abdominal aortic aneurysm wall. *J Vasc Surg.* 2003.
32. Andersen CB et al. AAA growth associated with high concentrations of plasma proteins in ILT and diseased arterial tissue. *Arterioscler Thromb Vasc Biol.*2018.
33. Stenbaek J et al. Growth of thrombus may be a better predictor of rupture than diameter in patients with abdominal aortic aneurysms. *Eur J Vasc Endovasc Surg.* 2000.
34. Speelman L et al. The mechanical role of thrombus on the growth rate of an abdominal aortic aneurysm. *J Vasc Surg.* 2010.
35. Domonkos A et al. Effect of intraluminal thrombus on growth rate of abdominal aortic aneurysms. *Int Angiol.* 2018.
36. Martufi G et al. Wall stress and thrombus thickness influence the local growth of AAA. *J Endovasc Ther.* 2016.
37. Barrett HE et al. On the influence of wall calcification and intraluminal thrombus on prediction of abdominal aortic aneurysm rupture. *J Vasc Surg.* 2018.
38. Haller SJ et al. Intraluminal thrombus is associated with early rupture of abdominal aortic aneurysm. *J Vasc Surg.* 2018.
39. Mower W et al. Effect of intraluminal thrombus on local abdominal aortic aneurysm wall strength. Annual International Conference of the IEEE Engineering in Medicine and Biology. 1999.
40. Metaxa E et al. Correlation of intraluminal thrombus deposition, biomechanics, and hemodynamics with surface growth and rupture in abdominal aortic aneurysm-Application in a clinical paradigm. *Ann Vasc Surg.* 2018.
41. Falcinelli E et al. Platelets release active matrix metalloproteinase-2 in vivo in humans at a site of vascular injury: Lack of inhibition by aspirin. *Br J Haematol.* 2007.
42. Sakalihasan N et al. Activated forms of MMP2 and MMP9 in abdominal aortic aneurysms. *J Vasc Surg.* 1996.
43. Kurosawa K et al. Current status of medical treatment for abdominal aortic aneurysm. *Circ J.*2013.

44. Pauling L et al. Collagenolytic activity in amphibian tissues: A tissue culture assay. *Biochim. et Biophys. Acta.* 1961.
45. Wang X et al. Matrix Metalloproteinases, vascular remodeling, and vascular disease. *Adv Pharmacol.* 2018.
46. Dean RA et al. Proteomics discovery of metalloproteinase substrates in the cellular context by iTRAQ™ labeling reveals a diverse MMP-2 substrate degradome. *Mol Cell Proteomics.* 2007;
47. Maguire EM et al. Matrix metalloproteinase in abdominal aortic aneurysm and aortic dissection. *Pharmaceuticals.* 2019.
48. Visse R et al. Matrix metalloproteinases and tissue inhibitors of metalloproteinases: Structure, function, and biochemistry. *Circ Res.* 2003.
49. Cui JZ et al. In vivo characterization of doxycycline-mediated protection of aortic function and structure in a mouse model of Marfan syndrome-associated aortic aneurysm. *Sci Rep.* 2019.
50. Raffetto JD et al. Matrix metalloproteinases and their inhibitors in vascular remodeling and vascular disease. *Biochem Pharmacol.* 2008.
51. Davis V et al. Matrix metalloproteinase-2 production and its binding to the matrix are increased in abdominal aortic aneurysms. *Arterioscler Thromb Vasc Biol.* 1998.
52. Thompson RW et al. Production and localization of 92-kilodalton gelatinase in abdominal aortic aneurysms. An elastolytic metalloproteinase expressed by aneurysm-infiltrating macrophages. *J Clin Invest.* 1995.
53. Hackmann AE et al. A randomized, placebo-controlled trial of doxycycline after endoluminal aneurysm repair. *J Vasc Surg.* 2008.
54. Wilson WRW et al. Elevated plasma MMP1 and MMP9 are associated with abdominal aortic aneurysm rupture. *Eur J Vasc Endovasc Surg.* 2008.
55. Hovsepian DM et al. Elevated plasma levels of matrix metalloproteinase-9 in patients with abdominal aortic aneurysms: A circulating marker of degenerative aneurysm disease. *J Vasc Interv Radiol.* 2000.
56. Sangiorgi G et al. Plasma levels of metalloproteinases-3 and -9 as markers of successful abdominal aortic aneurysm exclusion after endovascular graft treatment. *Circulation.* 2001.
57. Chew DKW et al. Matrix metalloproteinase-specific inhibition of Ca²⁺ entry mechanisms of vascular contraction. *J Vasc Surg.* 2004.

58. Pyo R et al. Targeted gene disruption of matrix metalloproteinase-9 (gelatinase B) suppresses development of experimental abdominal aortic aneurysms. *J Clin Invest.* 2000.
59. Matthew Longo G et al. Matrix metalloproteinases 2 and 9 work in concert to produce aortic aneurysms. *J Clin Invest.* 2002.
60. Giachelli CM et al. Osteopontin: a versatile regulator of inflammation and biomineralization. *Matrix Biol.* 2000.
61. Senger DR et al. Transformed mammalian cells secrete specific proteins and phosphoproteins. *Cell.* 1979.
62. O'Regan A et al. Osteopontin: A key cytokine in cell-mediated and granulomatous inflammation. *Int J Exp Pathol.* 2000.
63. Denhardt DT et al. Osteopontin as a means to cope with environmental insults: Regulation of inflammation, tissue remodeling, and cell survival. *J Clin Invest.* 2001.
64. Wei R et al. Osteopontin - A promising biomarker for cancer therapy. *J Cancer.* 2017.
65. Senger DR et al. A secreted phosphoprotein marker for neoplastic transformation of both epithelial and fibroblastic cells. *Nature.* 1983.
66. Gao YA et al. Expression and characterization of recombinant osteopontin peptides representing matrix metalloproteinase proteolytic fragments. *Matrix Biol.* 2004.
67. Christensen B et al. Osteopontin is cleaved at multiple sites close to its integrin-binding motifs in milk and is a novel substrate for plasmin and cathepsin D. *J Biol Chem.* 2010.
68. Golledge J et al. Association between osteopontin and human abdominal aortic aneurysm. *Arterioscler Thromb Vasc Biol.* 2007.
69. Schultz G et al. Enhanced abdominal aortic aneurysm formation in thrombin-activatable procarboxypeptidase B-deficient mice. *Arterioscler Thromb Vasc Biol.* 2010.
70. Yokosaki Y et al. Distinct structural requirements for binding of the integrins $\alpha\beta6$, $\alpha\beta3$, $\alpha\beta5$, $\alpha5\beta1$ and $\alpha9\beta1$ to osteopontin. *Matrix Biol.* 2005.
71. Agnihotri R et al. Osteopontin, a novel substrate for matrix metalloproteinase-3 (Stromelysin-1) and matrix metalloproteinase-7 (Matrilysin). *J Biol Chem.* 2001.

72. Takafuji V et al. An osteopontin fragment is essential for tumor cell invasion in hepatocellular carcinoma. *Oncogene*. 2007.
73. Philip S et al. Osteopontin stimulates tumor growth and activation of promatrix metalloproteinase-2 through nuclear factor- κ B-mediated induction of membrane type 1 matrix metalloproteinase in murine melanoma cells. *J Biol Chem*. 2001.
74. Seo KW et al. Mechanical stretch enhances the expression and activity of osteopontin and MMP-2 via the Akt1/AP-1 pathways in VSMC. *J Mol Cell Cardiol*. 2015.
75. Liu J et al. Mechanism of inhibition of matrix metalloproteinase-2 expression by doxycycline in human aortic smooth muscle cells. *J Vasc Surg*. 2003.
76. Lindeman JH et al. Clinical trial of doxycycline for matrix metalloproteinase-9 inhibition in patients with an abdominal aneurysm: doxycycline selectively depletes aortic wall neutrophils and cytotoxic T cells. *Circulation*. 2009.
77. Kazes I et al. Platelet release of trimolecular complex components MT1-MMP/TIMP2/MMP2: Involvement in MMP2 activation and platelet aggregation. *Blood*. 2000.
78. Koole D et al. Intraluminal abdominal aortic aneurysm thrombus is associated with disruption of wall integrity. *J Vasc Surg*. 2013.
79. Park EK et al. Optimized THP-1 differentiation is required for the detection of responses to weak stimuli. *Inflamm Res*. 2007.
80. Tajhya RB et al. Detection of matrix metalloproteinases by zymography. *Methods Mol Biol*. 2018.
81. Mylonas SN et al. Arterial stiffness assessed by cardio-ankle vascular index in patients with abdominal aortic aneurysm and its alterations after treatment. *Vasc Endovascular Surg*. 2021.
82. Gregory A et al. Non-invasive determination of aortic mechanical properties and their effects on left ventricular function following endovascular abdominal aneurysm repair. *J Med Biol Eng*. 2019.
83. Kanzaki H. Aortic compliance and left ventricular diastolic function. *Circ J*. 2014.
84. Qian W et al. Microskeletal stiffness promotes aortic aneurysm by sustaining pathological vascular smooth muscle cell mechanosensation via Piezo1. *Nat Commun*. 2022.
85. Åström Malm I et al. Increased arterial stiffness in males with abdominal aortic aneurysm. *Clin Physiol Funct Imaging*. 2021.

86. Di Achille P et al. A haemodynamic predictor of intraluminal thrombus formation in abdominal aortic aneurysms. *Proc R Soc A*. 2014.
87. Milne AA et al. Effects of asymptomatic abdominal aortic aneurysm on the soluble coagulation system, platelet count and platelet activation. *Eur J Vasc Endovasc Surg*. 1999.
88. Aslan JE. Platelet proteomes, pathways, and phenotypes as informants of vascular wellness and disease. *Arterioscler Thromb Vasc Biol*. 2021.
89. Alkarithi G et al. Thrombus structural composition in cardiovascular disease. *Arterioscler Thromb Vasc Biol*. 2021.
90. Mandel J et al. Beyond hemostasis: Platelet innate immune interactions and thromboinflammation. *Int J Mol Sci*. 2022.
91. Zhu C et al. Intraluminal thrombus predicts rapid growth of abdominal aortic aneurysms. *Radiology*. 2020.
92. Vande Geest JP et al. Towards a noninvasive method for determination of patient-specific wall strength distribution in abdominal aortic aneurysms. *Ann Biomed Eng*. 2006.
93. Golledge J et al. Association of oral anticoagulation prescription with clinical events in patients with an asymptomatic unrepaired abdominal aortic aneurysm. *Biomedicines*. 2022.
94. Sun W et al. Targeting platelet activation in abdominal aortic aneurysm: Current knowledge and perspectives. *Biomolecules*. 2022.
95. Houard X et al. Mediators of neutrophil recruitment in human abdominal aortic aneurysms. *Cardiovasc Res*. 2009.
96. Owens AP et al. Platelet inhibitors reduce rupture in a mouse model of established abdominal aortic aneurysm. *Arterioscler Thromb Vasc Biol*. 2015.
97. Li T et al. The elevated expression of TLR4 and MMP9 in human abdominal aortic aneurysm tissues and its implication. *BMC Cardiovasc Disord*. 2021.
98. Weiss D et al. Biomechanical consequences of compromised elastic fiber integrity and matrix cross-linking on abdominal aortic aneurysmal enlargement. *Acta Biomater*. 2021.
99. Jones B et al. Structurally abnormal collagen fibrils in abdominal aortic aneurysm resist platelet adhesion. *J Thromb Haemost*. 2022.
100. Vorp DA et al. Association of intraluminal thrombus in abdominal aortic aneurysm with local hypoxia and wall weakening. *J Vasc Surg*. 2001.

101. Vorp DA et al. Effect of intraluminal thrombus thickness and bulge diameter on the oxygen diffusion in abdominal aortic aneurysm. *J Biomech Eng.* 1998.
102. Simões G et al. Matrix metalloproteinases in vascular pathology. *Microvasc Res.* 2022.
103. Liu Y et al. MMP-2 and MMP-9 contribute to the angiogenic effect produced by hypoxia/15-HETE in pulmonary endothelial cells. *J Mol Cell Cardiol.* 2018.
104. Polzer S et al. The impact of intraluminal thrombus failure on the mechanical stress in the wall of abdominal aortic aneurysms. *Eur J Vasc Endovasc Surg.* 2011.
105. Hattori T et al. Both full-length and protease-cleaved products of osteopontin are elevated in infectious diseases. *Biomedicines.* 2021.
106. Icer MA et al. The multiple functions and mechanisms of osteopontin. *Clin Biochem.* 2018.
107. Schuch K et al. Osteopontin affects macrophage polarization promoting endocytic but not inflammatory properties. *Obesity (Silver Spring).* 2016.
108. Myles T et al. Thrombin activatable fibrinolysis inhibitor, a potential regulator of vascular inflammation. *J Biol Chem.* 2003.
109. Dale MA et al. Inflammatory cell phenotypes in AAAs: Their role and potential as targets for therapy. *Arterioscler Thromb Vasc Biol.* 2015.
110. Scatena M et al. Osteopontin: a multifunctional molecule regulating chronic inflammation and vascular disease. *Arterioscler Thromb Vasc Biol.* 2007.
111. Inada K et al. Moxifloxacin induces aortic aneurysm and dissection by increasing osteopontin in mice. *Biochem Biophys Res Commun.* 2022.
112. Fan F et al. Osteopontin in the pathogenesis of aortic dissection by the enhancement of MMP expressions. *Int Heart J.* 2019.
113. Anbarasen L et al. Expression of osteopontin, matrix metalloproteinase-2 and -9 proteins in vascular instability in brain arteriovenous malformation. *PeerJ.* 2019.
114. Singh M et al. Osteopontin: Role in extracellular matrix deposition and myocardial remodeling post-MI. *J Mol Cell Cardiol.* 2010.
115. Isoda K et al. Osteopontin plays an important role in the development of medial thickening and neointimal formation. *Circ Res.* 2002.
116. Mi T et al. The elevated expression of osteopontin and NF- κ B in human aortic aneurysms and its implication. *J Huazhong Univ Sci Technolog Med Sci.* 2011.

117. Freestone T et al. Inflammation and matrix metalloproteinases in the enlarging abdominal aortic aneurysm. *Arterioscler Thromb Vasc Biol.* 1995.
118. Bendeck MP et al. Smooth muscle cell matrix metalloproteinase production is stimulated via alpha(v) beta(3) integrin. *Arterioscler Throb Vasc Biol.* 2000.
119. Lindsey M et al. Osteopontin is proteolytically processed by matrix metalloproteinase 9. *Can J Physiol Pharmacol.* 2015.
120. Lai CF et al. OPN-NADPH Oxidase signaling cascade promotes pro-MMP9 activity. *Circ Res.* 2006.
121. Powell MA et al. Matrix metalloproteinase 9 and osteopontin interact to support synaptogenesis in the olfactory bulb after mild traumatic brain injury. *J Neurotrauma.* 2019.
122. Cai D et al. A novel mechanism underlying inflammatory smooth muscle phenotype in abdominal aortic aneurysm. *Circ Res.* 2021.
123. Jiang L et al. Calpain-1 regulation of matrix metalloproteinase 2 activity in vascular smooth muscle cells facilitates age-associated aortic wall calcification and fibrosis. *Hypertension.* 2012.
124. McNulty M et al. Aging is associated with increased matrix metalloproteinase-2 activity in the human aorta. *Am J Hypertens.* 2005.
125. Jana S et al. Extracellular matrix, regional heterogeneity of the aorta, and aortic aneurysm. *Exp Mol Med.* 2019.
126. Huusko T et al. Elevated messenger RNA expression and plasma protein levels of osteopontin and matrix metalloproteinase types 2 and 9 in patients with ascending aortic aneurysms. *J Thorac Cardiovasc Surg.* 2013.
127. Sakalihasan N et al. Modifications of the extracellular matrix of aneurysmal abdominal aortas as a function of their size. *Eur J Vasc Surg.* 1993.
128. Cavinato C et al. Evolving structure-function relations during aortic maturation and aging revealed by multiphoton microscopy. *Mech Ageing Dev.* 2021.
129. Cavinato C et al. Progressive microstructural deterioration dictates evolving biomechanical dysfunction in the Marfan aorta. *Front Cardiovasc Med.* 2021.
130. Dale MA et al. Elastin-derived peptides promote abdominal aortic aneurysm formation by modulating M1/M2 macrophage polarization. *J Immunol.* 2016.
131. Golledge J et al. Circulating markers of abdominal aortic aneurysm presence and progression. *Circulation.* 2008.

132. Farrokhi V et al. Assessing the feasibility of neutralizing osteopontin with various therapeutic antibody modalities. *Sci Rep.* 2018.